LIMNOLOGY and OCEANOGRAPHY

ASLO

Limnol. Oceanogr. 64, 2019, 1716–1736

doi: 10.1002/lno.11147

Impact of ocean acidification and high solar radiation on productivity and species composition of a late summer phytoplankton community of the coastal Western Antarctic Peninsula

Jasmin P. Heiden,[1,2] Christian Völkner,[1] Elizabeth M. Jones,[3,4,5] Willem H. van de Poll,[3] Anita G. J. Buma,[3] Michael P. Meredith,[6] Hein J. W. de Baar,[3,4] Kai Bischof,[2] Dieter Wolf-Gladrow,[1] Scarlett Trimborn [1,2*]

[1]Alfred-Wegener-Institut Helmholtz Zentrum für Polar- und Meeresforschung (AWI), Bremerhaven, Germany
[2]Marine Botany, University of Bremen, Bremen, Germany
[3]Department of Ocean Ecosystems, Energy and Sustainability Research Institute Groningen, University of Groningen, Groningen, The Netherlands
[4]NIOZ Royal Netherlands Institute for Sea Research and Utrecht University, Den Burg, The Netherlands
[5]Institute for Marine Research, Fram Centre, Tromsø, Norway
[6]British Antarctic Survey, Cambridge, UK

Abstract

The Western Antarctic Peninsula (WAP), one of the most productive regions of the Southern Ocean, is currently undergoing rapid environmental changes such as ocean acidification (OA) and increased daily irradiances from enhanced surface-water stratification. To assess the potential for future biological CO_2 sequestration of this region, we incubated a natural phytoplankton assemblage from Ryder Bay, WAP, under a range of pCO_2 levels (180 μatm, 450 μatm, and 1000 μatm) combined with either moderate or high natural solar radiation (MSR: 124 μmol photons m^{-2} s^{-1} and HSR: 435 μmol photons m^{-2} s^{-1}, respectively). The initial and final phytoplankton communities were numerically dominated by the prymnesiophyte *Phaeocystis antarctica*, with the single cells initially being predominant and solitary and colonial cells reaching similar high abundances by the end. Only when communities were grown under ambient pCO_2 in conjunction with HSR did the small diatom *Fragilariopsis pseudonana* outcompete *P. antarctica* at the end of the experiment. Such positive light-dependent growth response of the diatom was, however, dampened by OA. These changes in community composition were caused by an enhanced photosensitivity of diatoms, especially *F. pseudonana*, under OA and HSR, reducing thereby their competitiveness toward *P. antarctica*. Moreover, community primary production (PP) of all treatments yielded similar high rates at the start and the end of the experiment, but with the main contributors shifting from initially large to small cells toward the end. Even though community PP of Ryder Bay phytoplankton was insensitive to the changes in light and CO_2 availability, the observed size-dependent shift in productivity could, however, weaken the biological CO_2 sequestration potential of this region in the future.

Increasing emissions of carbon dioxide (CO_2) into the atmosphere from anthropogenic sources result in increased CO_2 uptake of the world's oceans (IPCC 2014). Due to a higher solubility of CO_2 at low seawater temperatures, the projected rise in CO_2 is expected to have greater influences in polar oceans (Orr et al. 2005). As a consequence, concentrations of true aqueous CO_2 in seawater are expected to double by the end of this century (Zeebe and Wolf-Gladrow 2001; IPCC 2014). Coastal waters of the Western Antarctic Peninsula (WAP) represent an efficient sink for atmospheric CO_2, which is largely driven by biological production (Arrigo et al. 2008; Legge et al. 2015; Jones et al. 2017), accounting for 745 mg C m^{-2} d^{-1} (Vernet et al. 2008) compared to the less productive pelagic waters of the Southern Ocean (148 mg C m^{-2} d^{-1}, Arrigo et al. 2008). In recent years, warming of surface waters and increased regional wind speeds have occurred contemporaneously with a shortening of the sea ice season along the WAP (Meredith and King 2005; Ducklow et al. 2007; Turner et al. 2013), with low ice winters being followed by reduced primary productivity during summer (Venables et al. 2013; Rozema et al. 2017*a*). In particular, the northern part of the WAP was found to be less productive over the past three decades (Montes-Hugo et al. 2009; Hyewon et al. 2018). Increasing heat flux to the ocean and strong freshwater

*Correspondence: scarlett.trimborn@awi.de

inputs from melting glaciers and sea ice can act to strengthen stratification and reduce mixed layer depths in coastal regions, though mechanical mixing by winds can counter this, with the balance being dependent on local meteorological conditions and processes. Nonetheless, changes in mixing and sea ice cover are expected to alter primary productivity in the coastal and open-shelf regions of the WAP (Legge et al. 2015) and given the importance of the WAP in overall productivity, it is critical to assess how ocean acidification (OA) and changes in overall light availability will alter the productivity of this region.

Diatoms and the prymnesiophyte *Phaeocystis antarctica* are the dominant phytoplankton along the WAP (DiTullio and Smith 1996; Arrigo et al. 1999, 2000; Smith and Asper 2001; Garibotti et al. 2003; Annett et al. 2010; Rozema et al. 2017*a*) and shifts toward one of the two groups have strong implications for future biogeochemical cycling. Previous studies revealed a dominance of *P. antarctica* in deep mixed waters with low light conditions and of diatoms in the more stratified waters with higher daily irradiances (DiTullio and Smith 1996; Arrigo et al. 1999, 2000; Sweeney et al. 2000; Smith and Asper 2001; Annett et al. 2010; Rozema et al. 2017*a*). The predicted increase of seawater surface temperatures and related sea ice melt will tend to enhance stratification, exposing coastal Antarctic phytoplankton to higher daily integrated irradiances, thus likely promoting diatom abundance (Arrigo et al. 1999; Boyd et al. 2015), though changes in wind-induced upper-ocean mixing could counter this to some extent. During a shipboard incubation experiment with a natural phytoplankton community from the Ross Sea, increased natural daily irradiances did not alter particulate organic carbon (POC) formation, but led to lowered abundance of diatoms relative to *P. antarctica* (Feng et al. 2010). Consistent with this, a high tolerance of temperate and Antarctic *Phaeocystis* strains to different constant or dynamic daily integrated irradiances (65–200 μmol photons m^{-2} s^{-1}) was previously reported, indicating no negative impacts of strong light on either growth or carbon fixation (Moisan and Mitchell 1999; Arrigo et al. 2010; Hoogstraten et al. 2012*a*; Trimborn et al. 2017*a*). These findings contradict the proposed shift from a dominance of *P. antarctica* toward diatoms in a more stratified future ocean (Arrigo et al. 1999).

Several incubation studies revealed that OA influence natural phytoplankton assemblages of the Southern Ocean (SO), both in terms of community structure and/or productivity (Tortell et al. 2008; Feng et al. 2010; Hoppe et al. 2013; Davidson et al. 2016; Thomson et al. 2016; Trimborn et al. 2017*b*; Hancock et al. 2018), with only few studies reporting no such changes (McMinn et al. 2014; Young et al. 2015; Coad et al. 2016). Unfortunately, most of these studies were conducted under constant light, thus neglecting the fact that exposure of phytoplankton to a naturally fluctuating light regime was found to be more stressful, hence impacting growth and carbon production (Wagner et al. 2006; Boelen et al. 2011; Su et al. 2012; Hoppe et al. 2015). How increased solar radiation in conjunction with OA affects phytoplankton growth and productivity has not yet been assessed for phytoplankton of WAP waters. To date, information just exists for a mixed phytoplankton community from the Ross Sea, which showed a shift from a dominance of *Cylindrotheca* toward *Chaetoceros* accompanied by a decrease of the maximum photochemical yield, indicating lowered physiological fitness in response to both increased solar radiation and OA (Feng et al. 2010). In line with the latter study, elevated partial pressure of CO_2 (pCO_2) in conjunction with constant high irradiance resulted in light stress for several Antarctic diatom species in laboratory experiments (Hoppe et al. 2015; Heiden et al. 2016, 2018; Trimborn et al. 2017*a*) while *P. antarctica* remained unaffected (Trimborn et al. 2017*a*; Koch et al. 2019). In response to the projected rise in solar radiation and pCO_2, the competitiveness of the two taxa could potentially alter species distribution and ultimately the potential of biological carbon drawdown of coastal WAP waters. To better understand the interactive effects of OA and increased natural solar radiation on phytoplankton community composition, POC production and photophysiology of phytoplankton communities from Antarctic coastal waters, we conducted a combined CO_2-solar radiation experiment with a phytoplankton community from Ryder Bay, in the southern part of WAP, a region of strong climatic variability and change (Venables et al. 2013). Ryder Bay is the site of the Rothera Oceanographic and Biological Time Series (RaTS), one of the longest running year-round oceanographic monitoring stations in coastal Antarctica (Clarke et al. 2008).

Materials and methods

Culture conditions

On 11th February 2015, the phytoplankton community was sampled from the sea surface at the Rothera Time Series long-term monitoring site 1 (RaTS, 67° 34.20′ S, 68° 13.50′ W) in Ryder Bay, West Antarctic Peninsula (WAP) using a Niskin bottle rinsed with ambient seawater prior to sampling. On this day, irradiance was 130 μmol photons m^{-2} s^{-1} in surface water and the mixed layer depth was 8 m (data available at British Oceanographic Data Centre). The sampled seawater containing the community was immediately filtered through a cleaned 200 μm mesh to avoid presence of large grazers inside the 18 sterile 4-L polycarbonate bottles for incubation. An additional 150 L of seawater was sampled, sterile filtered (0.2 μm, AcroPak 1500, PALL) and stored at 0°C in the dark in sterile 10 L containers for later use as dilution seawater. The 18 incubation bottles were placed outdoors inside two acrylic glass incubators (115 × 65 × 65 cm) covered with neutral density light filters generating two distinct light conditions ~30% and ~10% of incident solar radiation referred to as moderate and high solar radiation treatment, respectively (MSR = 124 ± 50 μmol photons m^{-2} s^{-1} and HSR = 435 ± 197 μmol photons m^{-2} s^{-1}, Fig. 1). As the mean measured light intensity at the surface of the RaTS site was 180 ± 158 μmol photons

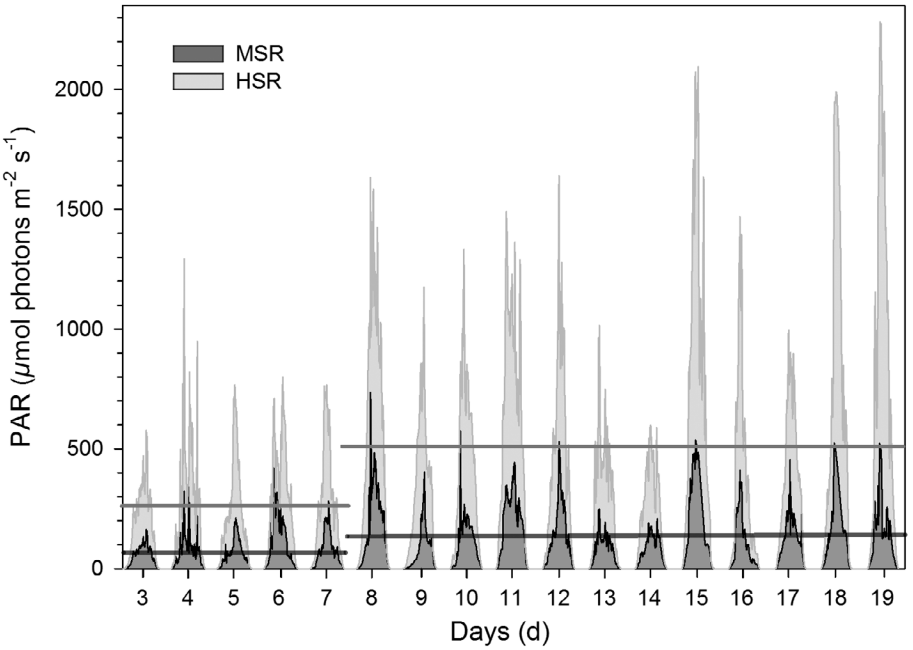

Fig. 1. From day 3 on, incident solar radiation was continuously recorded every 15 min over the whole experiment in two outdoor incubators, which were covered with ~30% and ~10% neutral density light filters generating two distinct light conditions of MSR and HSR (MSR = 124 ± 50 μmol photons m^{-2} s^{-1} and HSR = 435 ± 197 μmol photons m^{-2} s^{-1}, respectively). Lines indicate the mean daily irradiances over the two experimental phases of the MSR treatment in black and for the HSR treatment in dark gray. During the first experimental phase, which lasted until day 7, MSR and HSR treatments were exposed to a mean daily irradiance of 82 ± 24 μmol photons m^{-2} s^{-1} and 260 ± 43 μmol photons m^{-2} s^{-1}, respectively. During the second experimental phase after day 7, MSR and HSR was 141 ± 48 μmol photons m^{-2} s^{-1} and 508 ± 190 μmol photons m^{-2} s^{-1} on average per day.

m^{-2} s^{-1} in late summer (February and March) over the last 13 yr (from 2003 to 2015), the applied light conditions of the MSR treatment represent realistic natural conditions. To simulate increased daily irradiances from enhanced surface-water stratification, the elevated mean irradiance of the HSR treatment mimics future light conditions. To keep temperatures constant inside the incubators, incubation bottles were cooled by a flow-through of seawater from the adjacent Ryder Bay (0.1 ± 0.2°C). In addition to the two irradiance regimes, the triplicate incubation bottles were continuously bubbled with humidified air of either ambient (450 μatm, ambient pCO_2 treatment; using an air pump) or premixed-air (Air Liquide Deutschland, Düsseldorf, Germany) of low (180 μatm, low pCO_2 treatment) and elevated pCO_2 (1000 μatm, OA treatment) through sterile 0.2 μm air filters (Midisart 2000 Sartorius Stedim).

Initial concentrations of nitrogen (sum of nitrate and nitrite), phosphate, and silicate were 5.2 μM, 0.64 μM, and 45 μM, respectively. At the start of the first and second phase of the incubation experiment, phosphate was added to a final concentration of 1.6 μM phosphate to each incubation bottle. The phosphate addition allowed better resolution of phytoplankton growth indirectly from phosphate drawdown over the course of the whole experiment. To this end, 10 mL samples for the phosphate determination were taken from the incubation bottles every second day. As soon as phosphate concentrations were drawdown by ~0.6 μM in the incubation bottles, hence the same concentration at which the phytoplankton community was initially sampled, overall sampling took place to avoid any further reduction in phosphate concentration. Depending on the experimental treatment, after 5 d up to 7 d (5 d: 180 HSR and 450 HSR; 6 d: 1000 HSR and 180 MSR; 7 d: 450 MSR and 1000 MSR) all incubations were sampled apart from 200 mL, which were topped up with the previously sampled and filtered seawater (4000 mL) to maintain phytoplankton growth. In total, incubations were diluted once. We denote the experimental phases before and after dilution as the first and second experimental phase, respectively. In total, depending on experimental treatment the CO_2-solar radiation experiment lasted between 15 d and 19 d (15 d: 180 HSR and 450 HSR; 16 d: 1000 HSR; 18 d: 180 MSR; 19 d: 450 MSR and 1000 MSR). The experiment was conducted from February to March 2015 under a natural light–dark cycle of 16 : 8 h.

Monitoring of irradiance, temperature, and macronutrients

From day 3 onward, incident irradiance (Fig. 1) and temperature were continuously monitored in the flow-through seawater inside the two acrylic glass incubators covered with neutral density light filters using light (Odyssey Photosynthetic Irradiance Logger, Dataflow Systems PTY, Christchurch, New Zealand) and temperature (TidbiT, HOBO ware, Onset Computer Corporation, Bourne, U.S.A.) loggers. These recorded temperature and irradiance every 15 min over the whole duration of the experiment. Every second

day, phosphate concentrations in the experimental bottles were measured colorimetrically on-site following the method of Murphy and Riley (1962). An additional set of nutrient samples (phosphate, nitrate, nitrite, ammonium, and silicate) was taken at the start and the end of each experimental phase using sterile 0.2 μm syringe filters (Sartorius Stedium, Göttingen, Germany). All samples were frozen and stored at −20°C in 15 mL polycarbonate vials prior to analysis at the Alfred Wegener Institute, Germany. Prior to analysis, samples were defrosted over-night and then measured colorimetrically using a QuAAtro SFA Flow Injection Analyzer (Seal Analytical, Mequon, U.S.A.) following Grasshoff et al. (1983).

Seawater carbonate system

The pH was measured in all bubbled incubation and medium bottles every second day of the experiment using a pH-ion meter (826 pH mobile, Metrohm, Filderstadt, Germany), calibrated upon use (3-point calibration) with National Institute of Standards and Technology-certified buffer systems. Even though usage of the NBS scale and NIST buffers is not optimal for the determination of seawater pH (Zeebe and Wolf-Gladrow 2001), our three pCO_2 treatments (low, ambient, and high) resulted in three different pH values (~8.4, ~8.1, and ~7.7), varying at the most 0.05 pH units (Table 1). This means that the change of about 0.3 pH units between the three pCO_2 treatments is large when compared to the calculation error induced by the NBS scale and therefore should be negligible. Samples for total alkalinity (TA) were taken at the start and end of the two experimental phases. For this, seawater was filtered (GF/F glass fiber filters, ~0.6 mm, Whatman, Wisconsin, U.S.A.), poisoned with 0.03% $HgCl_2$, and stored at 4°C in 250 mL glass flasks. All TA samples were analyzed on-site using a VINDTA 3C (Versatile Instrument for the Determination of Total Alkalinity, Marianda, Kiel, Germany) following methods prescribed in Dickson et al. (2007). Determination of TA was done by automated potentiometric titration with 0.1 M hydrochloric acid (Dickson 1981). Accuracy was maintained by analysis of Certified Reference Material (CRM, batch 130) supplied by A. G. Dickson at Scripps Institute of Oceanography (San Diego, California) every 10–20 samples. The precision of the TA measurements was 1.5 μmol kg^{-1} based on the average difference between CRM in-bottle duplicate analyses. TA, pH, silicate, phosphate, temperature (0.5°C), and salinity (33.03) measurements were used to determine the seawater carbonate system using the CO2Sys program (Pierrot et al. 2006) and the equilibrium constant of Mehrbach et al. (1973) refitted by Dickson and Millero (1987).

Elemental composition

Samples for POC and particulate organic nitrogen (PON) were taken at the start and end of the two experimental phases. To compare the contributions of large (>20 μm) and small (<20 μm) phytoplankton to POC, samples were taken for the whole phytoplankton community as well as for the small phytoplankton fraction, which was passed through a 20 μm mesh. For determination of the elemental composition for

Table 1. Partial pressures of CO_2 (pCO_2) and dissolved inorganic carbon (DIC) concentrations were calculated from total alkalinity (TA), pH, silicate, phosphate, temperature, and salinity using the CO2Sys program (Pierrot et al. 2006). For all parameters, values are given for the incubation bottles at the start and after the two experimental phases of the natural phytoplankton community exposed to MSR and HSR in combination with low, ambient, and high pCO_2. Values represent the means (± SD) of triplicate incubations. Significant differences ($p < 0.05$) between treatments are indicated by + for light effects and # for pCO_2 effects.

Light treatment	pCO_2 treatment	pCO_2 calculated (μatm)	DIC calculated (μmol kg^{-1})	TA measured (μmol kg^{-1})	pH measured (NBS)
Start		181	2009	2252	8.42
End of first experimental phase:					
MSR	Low pCO_2	173 ± 5#	1993 ± 6#	2250 ± 6	8.44 ± 0.01#
	Ambient pCO_2	445 ± 12#	2144 ± 5#	2248 ± 7	8.08 ± 0.01#
	High pCO_2	1067 ± 81#	2247 ± 5#	2251 ± 3	7.73 ± 0.03#
HSR	Low pCO_2	165 ± 9#	1983 ± 15#	2249 ± 3	8.46 ± 0.02#
	Ambient pCO_2	428 ± 44#	2135 ± 8#	2249 ± 3	8.10 ± 0.04#
	High pCO_2	924 ± 43#	2233 ± 3#	2248 ± 1	7.78 ± 0.01#
End of second experimental phase:					
MSR	Low pCO_2	187 ± 8#	2000 ± 17#	2252 ± 8	8.42 ± 0.02#
	Ambient pCO_2	456 ± 8#	2151 ± 2#	2253 ± 1	8.07 ± 0.01#
	High pCO_2	978 ± 110#	2241 ± 17#	2251 ± 1	7.76 ± 0.05#
HSR	Low pCO_2	204 ± 7#	2020 ± 7#	2253 ± 2	8.38 ± 0.01#
	Ambient pCO_2	481 ± 16#	2154 ± 5#	2252 ± 1	8.05 ± 0.01#
	High pCO_2	1035 ± 69#	2249 ± 5#	2255 ± 5	7.74 ± 0.03#

both phytoplankton size classes, all samples were gently filtered (<20 mmHg) for POC and PON content onto precombusted glass-fiber filters (15 h, 200°C, GF/F ~0.6 μm, Whatman, Wisconsin, U.S.A.). All filters were stored at −20°C for later analysis at the Alfred Wegener Institute, Germany. Prior to analysis of POC and PON samples on an elemental analyzer (EURO EA Elemental Analyzer, Euro Vector, Redavalle, Italy), samples were defrosted (>12 h, 60°C), acidified with 0.1 mol HCl L^{-1}, and dried overnight (>12 h, 60°C). Contents of POC and PON were corrected for blank measurements and normalized to filtered volume. Taking into account the corresponding incubation time in days, net daily POC production rates were calculated.

Primary production

Size-fractionated primary production (PP) was determined at the start and the end of the two experimental phases. To compare between large (>20 μm) and small (<20 μm) phytoplankton, PP was determined for the whole phytoplankton community as well as for the small phytoplankton fraction, which was passed through a 20 μm mesh. For this, 10 mL of each size fraction was incubated in duplicates for 1 h at 100 μmol photons m^{-2} s^{-1} and 0°C after addition of a 10 mCi (0.37 MBq) spike of $NaH^{14}CO_3$ (PerkinElmer, 53.1 mCi $mmol^{-1}$). From the incubations, 50 μL aliquots were removed immediately and mixed with 10 mL of scintillation cocktail (Ultima Gold AB, Perkin Elmer) to determine the total amount of added $NaH^{14}CO_3$. For blank determination, another 50 μL of each seawater sample were removed, mixed with 500 μL 6 N HCl, to which 10 mL of scintillation cocktail were added. After 1 h incubation time, the reaction was terminated by addition of 500 μL 6 N HCl and samples left in the fume hood to degas for at least 24 h on a shaker table. After degassing, 10 mL of scintillation cocktail were added and vortexed. After ~2 h, samples were measured on a liquid scintillation counter (Tri-Carb2900TR, PerkinElmer) onsite. Carbon uptake rates were corrected for total dissolved inorganic carbon (DIC) concentrations and normalized to POC content of the respective size fraction.

Pigment analysis

Pigment samples were taken at the start and end of the two experimental phases. After gentle filtration onto glass fiber filters (<20 mmHg, GF/F ~0.6 μm, Whatman, Wisconsin, U.S.A.), samples were immediately frozen and stored at −80°C until analysis. Prior to analysis, filters were freeze dried for 48 h and pigments extracted in 90% acetone (v/v) for 48 h at 4°C in darkness. Total pigment concentrations (chlorophyll *a*, diadinoxanthin, and diatoxanthin) were determined via high-performance liquid chromatography (Waters 2695, Milford, U.S.A.) with a Zorbax Eclipse XDB-C8 column (3.5 μm particle size, Agilent Technologies, Santa Barbara, U.S.A.), using the method of Van Heukelem and Thomas (2001), modified after Perl (2009). Pigments were manually identified and quantified using pigment standard material (DHI Lab Products, Hoersholm, Denmark). All pigments were normalized to filtered volume. While chlorophyll *a* (Chl *a*) was normalized to POC content, the sum of diadinoxanthin (DD) and diatoxanthin (DT) was normalized to Chl *a*.

Phytoplankton community characterization

For determination of taxonomic phytoplankton composition, two aliquots of 200 mL of unfiltered seawater were preserved with either hexamine-buffered formalin solution (2% final concentration) or Lugol's solution (4% final concentration) at the start and the end of each experimental phase. Please note that samples of the low pCO_2 treatment of the end of the first experimental phase were lost and therefore their phytoplankton composition could not be characterized. All samples were stored at 4°C in the dark until further analysis via inverted light microscopy (Axiovert 200, Zeiss, Oberkochen, Germany). After sedimentation of 10 mL of sample for 24 h in sedimentation chambers (HydroBios, Kiel, Germany), phytoplankton species were enumerated according to the method of Utermöhl (1958) and the recommendations of Edler (1979). For each sample, in the aliquot, less abundant species were counted in the whole or half of the chamber. Highly abundant species were enumerated in at least two stripes, accounting for at least 400 cells. The phytoplankton species were identified according to taxonomic literature (Thomas et al. 1997). Numerically most abundant species were colonial *P. antarctica*, *Fragilariopsis* cf. *pseudonana*, *Fragilariopsis* cf. *curta*, *Fragilariopsis kerguelensis*, *Odontella* cf. *weissflogii*, *Eucampia* cf. *antarctica*, *Navicula* sp., *Pseudo-nitzschia* sp., and *Thalassiosira* cf. *antarctica*. In order to assess cell densities for colonial *P. antarctica*, the number of individual cells within colonies was counted by enumeration of all colonies and measurement of their size. To this end, an average number of cells for each colony size was determined using six different colony size categories (15–18 μm, 19–30 μm, 31–65 μm, 66–90 μm, 91–125 μm, and >126 μm) following Mathot et al. (2000). The total number of cells for each colony size category was then summed up to determine the total number of colonial *P. antarctica* cells per mL. Some flagellate species could not be identified, but were counted and all cell counts afterward combined in the group of unidentified flagellates. According to microscopic determination and counting, microzooplankton grazer abundance (<200 μm) remained unaltered in all treatments and at all sampling times of the incubation experiment. Based on cell counts, net accumulation rates (μ) of single-celled and colonial *P. antarctica*, of the small (<20 μm) and large (>20 μm) size fraction of diatoms and of *F. pseudonana* alone were calculated as:

$$\mu = (\ln N_{t2} - \ln N_{t1})/\Delta t \quad (1)$$

where N_{t1} and N_{t2} denote the cell abundances on the respective sampling days t_1 and t_2, and Δt is the corresponding incubation time in days.

Chl a fluorescence

Chl *a* fluorescence was measured with a Fast Repetition Rate fluorometer (FRRf, FastOcean PTX; Chelsea Technologies, West Molesey, UK) and a FastAct Laboratory system (Chelsea Technologies) at the start and end of the two experimental phases. Measurements were conducted at 0°C. Samples were dark-acclimated for at least 45 min prior to measurement. Excitation wavelength of the fluorometer's LEDs was 450 nm, 530 nm, and 624 nm with an automated adjustment of the light intensity (between 0.66×10^{22} and 1.2×10^{22}). The single turnover mode was used with 100 flashlets during the saturation phase on a 2 μs pitch and with 40 flashlets during the relaxation phase on a 50 μs pitch in order to cumulatively saturate PS II. Minimum (F_0) and maximum Chl *a* fluorescence (F_m) were based on iterative algorithms for induction (Kolber et al. 1998) and relaxation phase (Oxborough et al. 2012). After blank corrections with 0.22 μm filtered seawater, the maximum quantum yield of photochemistry in PSII (F_v/F_m, rel. unit) was calculated as:

$$F_v/F_m = (F_m - F_0)/F_m. \quad (2)$$

Additional Chl *a* fluorescence measurements were performed on every treatment in response to increasing incident irradiances (E, μmol photons m^{-2} s^{-1}) generating photosynthesis-irradiance-curves (PE-curves; irradiances ranged between 0 μmol photons m^{-2} s^{-1} and 1000 μmol photons m^{-2} s^{-1}) using seven steps with an acclimation duration of 5 min per light step and with six subsequent Chl *a* fluorescence measurements. From the fluorescence measurements, the light-adapted minimum (F') and maximum (F_m') fluorescence were derived to calculate the effective PSII quantum yield under ambient light (Genty et al. 1989).

$$F_q'/F_m' = (F_m' - F')/F_m' \quad (3)$$

Absolute electron transport rates (absETR, e^- $PSII^{-1}$ s^{-1}) were calculated from the functional absorption cross section of PSII (σ_{PSII}, nm^2 $PSII^{-1}$) and the incident irradiance E (Suggett et al. 2004, 2009) according to the following equation:

$$\text{absETR} = \sigma_{PSII} \times \left((F_q'/F_m')/(F_v/F_m) \right) \times E \quad (4)$$

A fit was applied to the irradiance-dependent absETRs following Ralph and Gademann (2005) with the use of SigmaPlot 13.0 software (SysStat Software), analyzing the following light-use characteristics: maximum light-use efficiency (α, rel. unit), minimum light saturation irradiance (I_K, μmol photons m^{-2} s^{-1}), and maximum absolute electron transport rate (ETR_m, e^- $PSII^{-1}$ s^{-1}). From the single turnover measurements of dark-adapted cells, the functional absorption cross section of PSII (σ_{PSII}, nm^2 $PSII^{-1}$), the time constant for electron transport at the acceptor side of PSII (τ_{Qa}, μs), and the connectivity factor (p, dimensionless) were derived according to Oxborough et al. (2012), using FastPro8 Software (Version 1.0.50, Kevin Oxborough, CTG).

Statistics

Combined effects of the different pCO_2 (low, ambient, and high) and solar radiation (MSR and HSR) conditions on experimental parameters were statistically analyzed using two-way ANOVA with Bonferroni's post hoc tests. Statistical analyses were performed using the program GraphPad Prism v.5.00 for Windows (Graph Pad Software). Significant differences were determined at the $\alpha = 0.05$ level. The dissimilarity analysis of phytoplankton community composition for the different treatments was performed according to Zuur et al. (2007). A dissimilarity index (DI) of 1.00 denotes 100% dissimilarity.

Results

Carbonate chemistry and macronutrient concentrations

At the time of sampling, seawater pCO_2 was 181 μatm and corresponded to a seawater pH of 8.42 (Table 1). During both experimental phases, carbonate chemistry remained constant with pH values of 8.43 ± 0.03, 8.08 ± 0.03, and 7.75 ± 0.03 and corresponding pCO_2 values of 182 ± 17 μatm, 455 ± 29 μatm, and 1016 ± 82 μatm in the low, ambient, and high pCO_2 treatments, respectively (Table 1). At the time of sampling of the phytoplankton community, solar radiation reached 130 μmol photons m^{-2} s^{-1} at the surface at the RaTS site 1. The mixed layer depth was 8 m. Over the duration of the first experimental phase, incubations were exposed to 82 ± 24 μmol photons m^{-2} s^{-1} and 260 ± 43 μmol photons m^{-2} s^{-1} on average per day in the MSR and HSR treatments, respectively (Fig. 1). The mean daily light intensity was higher in the second experimental phase with 141 ± 48 μmol photons m^{-2} s^{-1} and 508 ± 190 μmol photons m^{-2} s^{-1} in the MSR and HSR treatments, respectively (Fig. 1). Over the whole duration of experiment, the mean daily irradiance was 124 ± 50 μmol photons m^{-2} s^{-1} and 435 ± 197 μmol photons m^{-2} s^{-1} in the MSR and HSR treatments, respectively. The initial seawater contained 5.14 μM nitrate, 0.07 μM nitrite, 45 μM silicate, and 0.64 μM phosphate. At the start of both experimental phases, concentrations of phosphate accounted for 1.69 ± 0.09 μM. At the end of both experimental phases, concentrations of nitrate and nitrite were below detection limit in all treatments (data not shown), while concentrations of phosphate and silicate never fell below 0.78 μM and 37 μM, respectively (Table 2).

Elemental composition

The initial community had a carbon to nitrogen ratio (C : N) of 5.8 ± 0.1 mol mol^{-1} (Table 2). At the end of the first experimental phase, C : N ratios significantly increased from MSR to HSR in all pCO_2 treatments (two-way ANOVA: $p < 0.0001$). They were not affected by increasing pCO_2 in all light treatments except for the HSR treatment, which showed an enhancement by 22% from ambient to high pCO_2

Table 2. Ratios of carbon to nitrogen (C : N), net daily POC production rates, ratios of chlorophyll a to POC (Chl a : POC), the Chl a-based ratio of the light protective pigments diadino- and diatoxanthin (DD and DT, respectively; [DD + DT]:Chl a), concentrations of phosphate and silicate as well as cell numbers measured at the start and after the two experimental phases in a natural phytoplankton community exposed to MSR and HSR in combination with low, ambient, and high pCO_2. Cell count samples denoted by nd were lost and therefore could not be counted. Values represent the means (± SD) of triplicate incubations. Significant differences ($p < 0.05$) between treatments are indicated by + for light effects and # for pCO_2 effects.

Light treatment	pCO_2 treatment	C:N (mol mol^{-1})	POC production (μg C d^{-1})	Chl *a*:POC (g g^{-1})	(DD + DT): Chl *a* (g g^{-1})	Phosphate (μM)	Silicate (μM)	Cell number (cells mL^{-1})
Start		5.8 ± 0.1		0.009	0.06 ± 0.01	0.64	44.87	3290 ± 280
End of first experimental phase:								
MSR	Low pCO_2	7.0 ± 0.4^{+}	0.17 ± 0.02^{+}	0.016 ± 0.003^{+}	0.05 ± 0.01^{+}	0.78 ± 0.04	39.36 ± 0.64	nd
	Ambient pCO_2	7.6 ± 0.4^{+}	0.15 ± 0.01^{+}	0.014 ± 0.001^{+}	0.04 ± 0.01^{+}	0.85 ± 0.04	39.59 ± 0.82	7753 ± 1153
	High pCO_2	8.7 ± 0.8^{+}	0.16 ± 0.01^{+}	0.012 ± 0.001^{+}	0.06 ± 0.01^{+}	0.88 ± 0.03	40.75 ± 0.68	10,359 ± 1368
HSR	Low pCO_2	10.3 ± 1.3^{+}	0.26 ± 0.03^{+}	0.006 ± 0.001^{+}	0.12 ± 0.01^{+}	0.81 ± 0.03	40.22 ± 1.31	nd
	Ambient pCO_2	9.9 ± 0.7$^{+\#}$	0.25 ± 0.03^{+}	0.008 ± 0.001^{+}	0.12 ± 0.03^{+}	0.83 ± 0.10	41.28 ± 1.13	6624 ± 1386
	High pCO_2	12.1 ± 0.3$^{+\#}$	0.24 ± 0.01^{+}	0.006 ± 0.001^{+}	0.15 ± 0.01^{+}	0.82 ± 0.05	39.62 ± 0.50	9193 ± 1582
End of second experimental phase:								
MSR	Low pCO_2	10.8 ± 1.7	0.19 ± 0.01	0.009 ± 0.000	0.07 ± 0.00^{+}	0.84 ± 0.04	38.07 ± 0.28	15,403 ± 592
	Ambient pCO_2	7.6 ± 3.4	0.20 ± 0.01	0.008 ± 0.002	0.06 ± 0.01^{+}	0.89 ± 0.06	39.35 ± 1.46	14,866 ± 3001
	High pCO_2	11.2 ± 0.7	0.20 ± 0.01^{+}	0.008 ± 0.001	0.07 ± 0.02^{+}	0.92 ± 0.03	40.59 ± 1.15	14,590 ± 3043
HSR	Low pCO_2	11.8 ± 1.2	0.21 ± 0.01	0.006 ± 0.002	0.14 ± 0.03^{+}	0.80 ± 0.03	37.40 ± 1.19	17,381 ± 1627
	Ambient pCO_2	9.9 ± 0.9	0.21 ± 0.01	0.007 ± 0.001	0.12 ± 0.01^{+}	0.91 ± 0.01	39.06 ± 1.21	15,451 ± 762
	High pCO_2	11.7 ± 1.9	0.23 ± 0.01^{+}	0.006 ± 0.000	0.14 ± 0.02^{+}	0.90 ± 0.01	40.32 ± 0.52	11,415 ± 1175

(post hoc: $p < 0.05$). At the end of the experiment, C : N ratios were neither changed by the applied solar radiation regimes nor by pCO_2.

At the time of sampling, POC accounted for 394 ± 4 μg L^{-1}. At the end of the first experimental phase, daily POC production rates significantly increased between MSR and HSR (two-way ANOVA: $p < 0.0001$) (Table 2). During this phase, increasing pCO_2 had no effect on POC production rates. At the end of the experiment, POC production rates were neither changed by the applied solar radiation regimes nor by pCO_2, except for the high pCO_2 treatment, which showed a light-dependent stimulation by 13% (post hoc: $p < 0.05$) from MSR to HSR.

The Chl *a* concentration at the time of sampling was 3.5 ± 0.1 μg L^{-1}. When normalized to POC, the ratio of Chl *a* : POC accounted for 0.009 g g^{-1} initially (Table 2). After the first experimental phase, Chl *a* : POC significantly decreased from MSR to HSR in all pCO_2 treatments (two-way ANOVA: $p < 0.0001$). At the end of the experiment, increasing solar radiation did not affect Chl *a* : POC ratios in all pCO_2 treatments. There was no significant pCO_2 effect on Chl *a* : POC present after both experimental phases apart from the MSR treatment at the end of first experimental phase, where ratios significantly differed between low and high pCO_2 (25%, post hoc: $p < 0.05$).

At the start of the experiment, the ratio of the two light photoprotective pigments diadinoxanthin and diatoxanthin relative to Chl *a* ([DD + DT]:Chl *a*) was 0.06 ± 0.01 g g^{-1} (Table 2). After both experimental phases, (DD + DT):Chl *a* significantly increased from MSR to HSR in all pCO_2 treatments (two-way ANOVA: $p < 0.0001$). Increasing pCO_2 did not alter (DD + DT):Chl *a* in any solar radiation treatment.

Primary production

The initial PP rate of the whole phytoplankton community was 0.37 ± 0.06 μmol C (μmol POC)$^{-1}$ h^{-1}, with the large (>20 μm) and the small (<20 μm) phytoplankton size class accounting for 0.24 ± 0.05 μmol C (μmol POC)$^{-1}$ h^{-1} and 0.13 ± 0.02 μmol C (μmol POC)$^{-1}$ h^{-1}, respectively. At the end of the first experimental phase (Fig. 2a, c, e), PP rates of the large size fraction significantly declined from MSR to HSR in all pCO_2 treatments (two-way ANOVA: $p < 0.0001$, Fig. 2c) while rates of the small fraction remained unchanged under these conditions (Fig. 2e). In response to increasing pCO_2, PP rates of both size classes did generally not change except for the MSR treatments of the large size fraction, for which PP rates declined by 37% (post hoc: $p < 0.05$) between low and ambient pCO_2 (Fig. 2c). At the end of the second experimental phase, neither increasing solar radiation nor changes in pCO_2 altered PP rates of both size classes (Fig. 2b,d,f).

Community composition

Initially, the sampled phytoplankton community was with 57% ± 0% of all phytoplankton cells clearly dominated by *P. antarctica*, among the latter only 4% ± 2% were present in colonial form (Fig. 3). About 36% ± 1% of the community remained unidentified, belonging to other flagellates such as dinophyta and

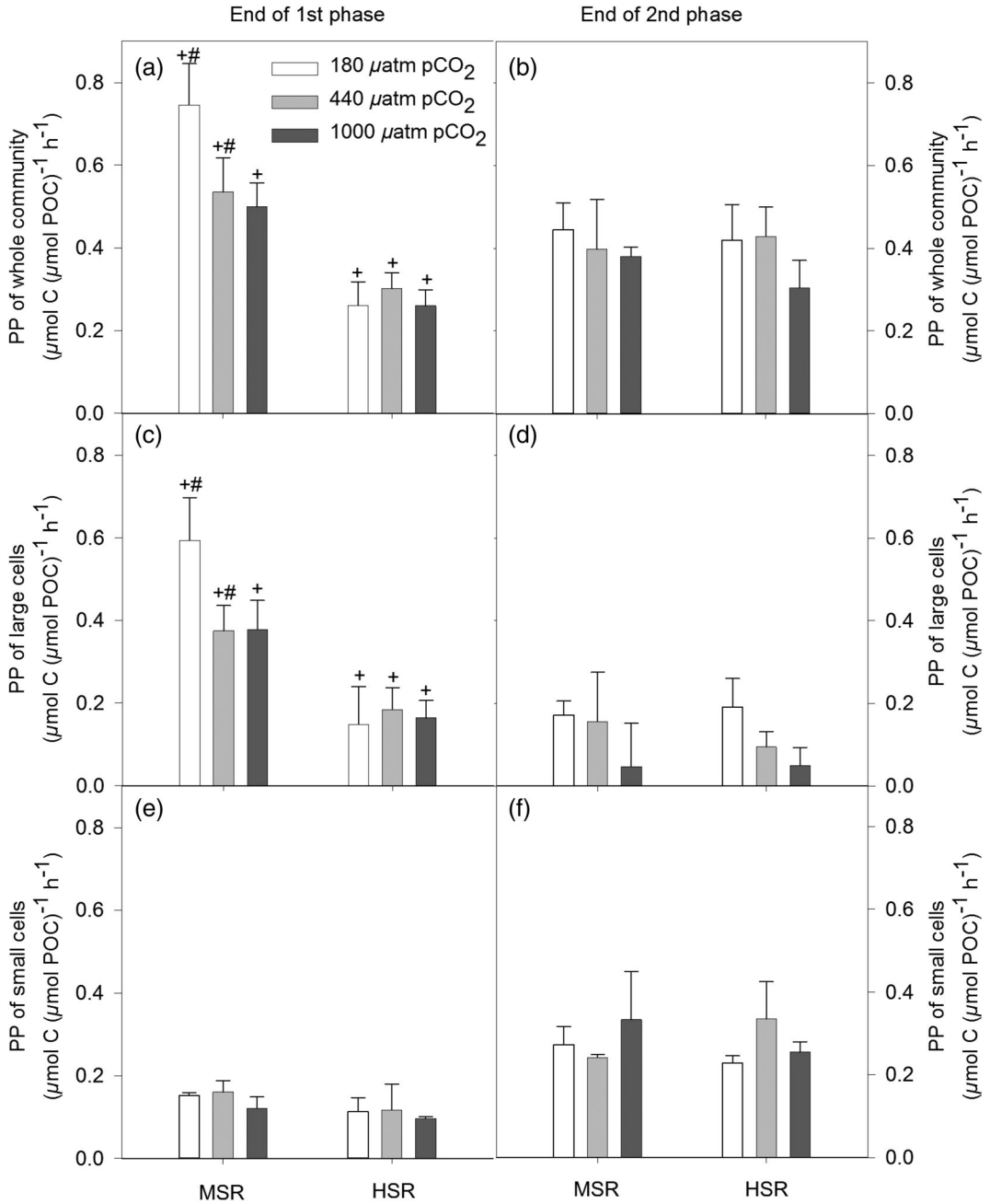

Fig. 2. Net PP rates (µmol C [µmol POC]$^{-1}$ h^{-1}) of the whole community (**a**, **b**), of large (>20 µm; **c**, **d**) and small (<20 µm; **e**, **f**) cells from a natural phytoplankton community after the first (**a**, **c**, **e**) and the second (**b**, **d**, **f**) experimental phase after exposure to MSR and HSR in combination with low, ambient, and high pCO_2. Values represent the means (± SD) of triplicate incubations. Significant differences ($p < 0.05$) between treatments are indicated by + for light effects and # for pCO_2 effects.

cryptophyta while diatoms made up only 7% ± 1% of the whole community. Among the latter, the genus *Fragilariopsis* contributed up to 65% ± 7% (*F. pseudonana*: 42% ± 6%, *F. kerguelensis*: 13% ± 3%, and *F. curta*: 10% ± 2% of all diatom cells), followed by 14% ± 2% of the genus *Odontella* sp., 5% ± 1% of *Pseudo-nitzschia* sp., and 5% ± 1% of *Eucampia* sp. At the end of the first experiment phase, the community composition was similar among the different applied light (ambient pCO_2 treatment: DI = 0.09; high pCO_2 treatment: DI = 0.10) and pCO_2 treatments (MSR treatment: DI = 0.10; HSR treatment: DI = 0.09). *P. antarctica* still dominated all treatments, accounting for 63–76%, with most cells occurring in the solitary cell form (Fig. 3). Among the community, diatoms made up between 9% and 13% among the different CO_2-light treatments, with *F. pseudonana* being

the most abundant species. In comparison to the start of the experiment, the relative contribution of *F. pseudonana* doubled in all treatments. Between 15% and 23% of the whole community in all treatments were other flagellate species.

At the end of the experiment, phytoplankton community composition was similar between MSR and HSR treatments (low pCO_2 treatment: DI = 0.18; ambient pCO_2 treatment: DI = 0.16; high pCO_2 treatment: DI = 0.12). Increasing pCO_2, however, differently affected final phytoplankton composition depending on the applied light regime. While final phytoplankton community structure was similar at MSR in response to increasing pCO_2 levels (low to ambient pCO_2: DI = 0.11; ambient to high pCO_2: DI = 0.20), the combination with HSR, however, more strongly altered phytoplankton community composition (low to ambient pCO_2: DI = 0.29; ambient to high pCO_2: DI = 0.29). In fact, microscopic analysis reveals that except for the community grown at ambient pCO_2 in conjunction with HSR, the most abundant species of final phytoplankton communities was *P. antarctica* (46–62%), for which half of the cells were in the colonial form. The overall contribution of diatoms was significantly increased, accounting for 21 up to 36%, Fig. 3). Among diatoms, *F. pseudonana* was generally the most abundant species, reaching between 75 and 87%. Within these communities, other flagellate species accounted only for 7 up to 11%. Only the final phytoplankton community grown under ambient pCO_2 and HSR displayed a shift toward a dominance of diatoms (66% ± 15%) over *P. antarctica* (total: 25% ± 12%, among them 10% ± 0% single-celled and 15% ± 12% colonial cells). In this case, the diatom community was dominated by 90% ± 2% by *F. pseudonana*. Other flagellates were also present and accounted for 9% ± 2%.

At the end of the first experimental phase, accumulation rates of large- and small-sized diatoms as well as of *F. pseudonana* were neither altered by increasing solar radiation nor by changes in pCO_2 (Fig. 4a,c,e). At the end of the experiment, accumulation rates of the large diatom fraction were stimulated by 32% from MSR to HSR at ambient (post hoc: $p < 0.01$), but not at high

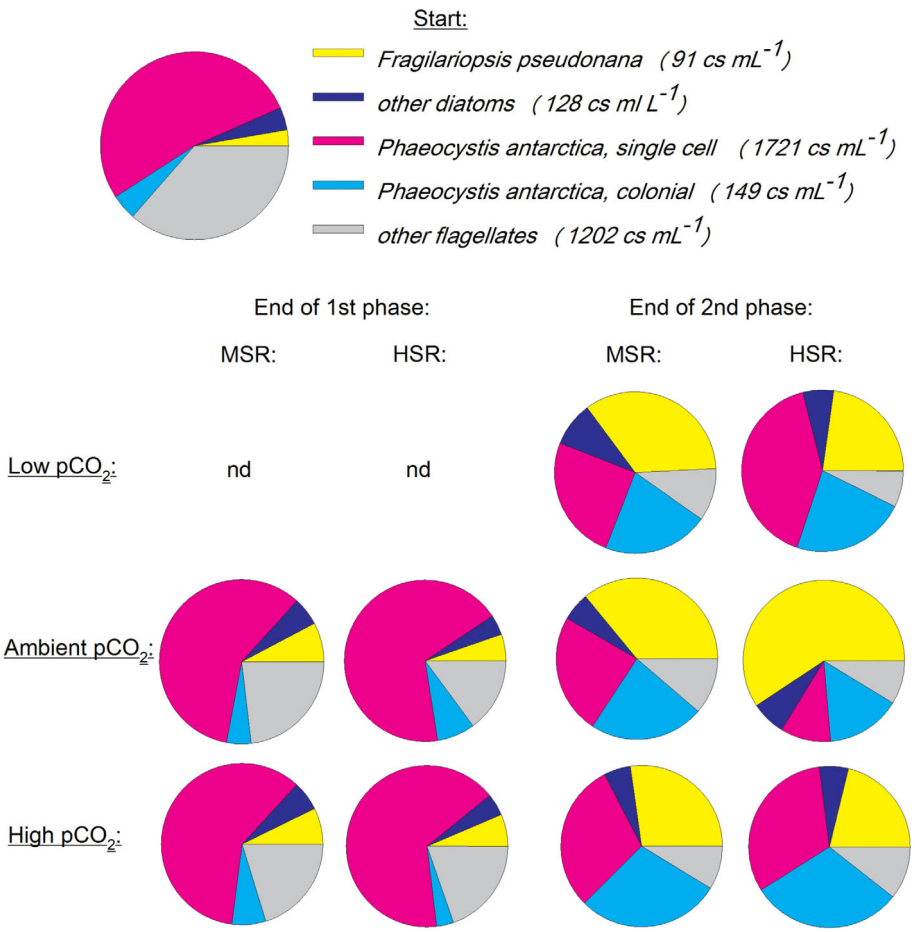

Fig. 3. Relative abundances of the dominant two phytoplankton species *P. antarctica* (single cell: pink, colonial: turquoise) and *F. pseudonana* (yellow), other diatoms (blue), and unidentified other flagellates (gray) at the start and the end of both experimental phases after exposure to MSR and HSR in combination with low, ambient, and high pCO_2. Please note that samples of the low pCO_2 treatment of the end of the first experimental phase were lost and therefore their phytoplankton composition could not be characterized, as indicated by nd.

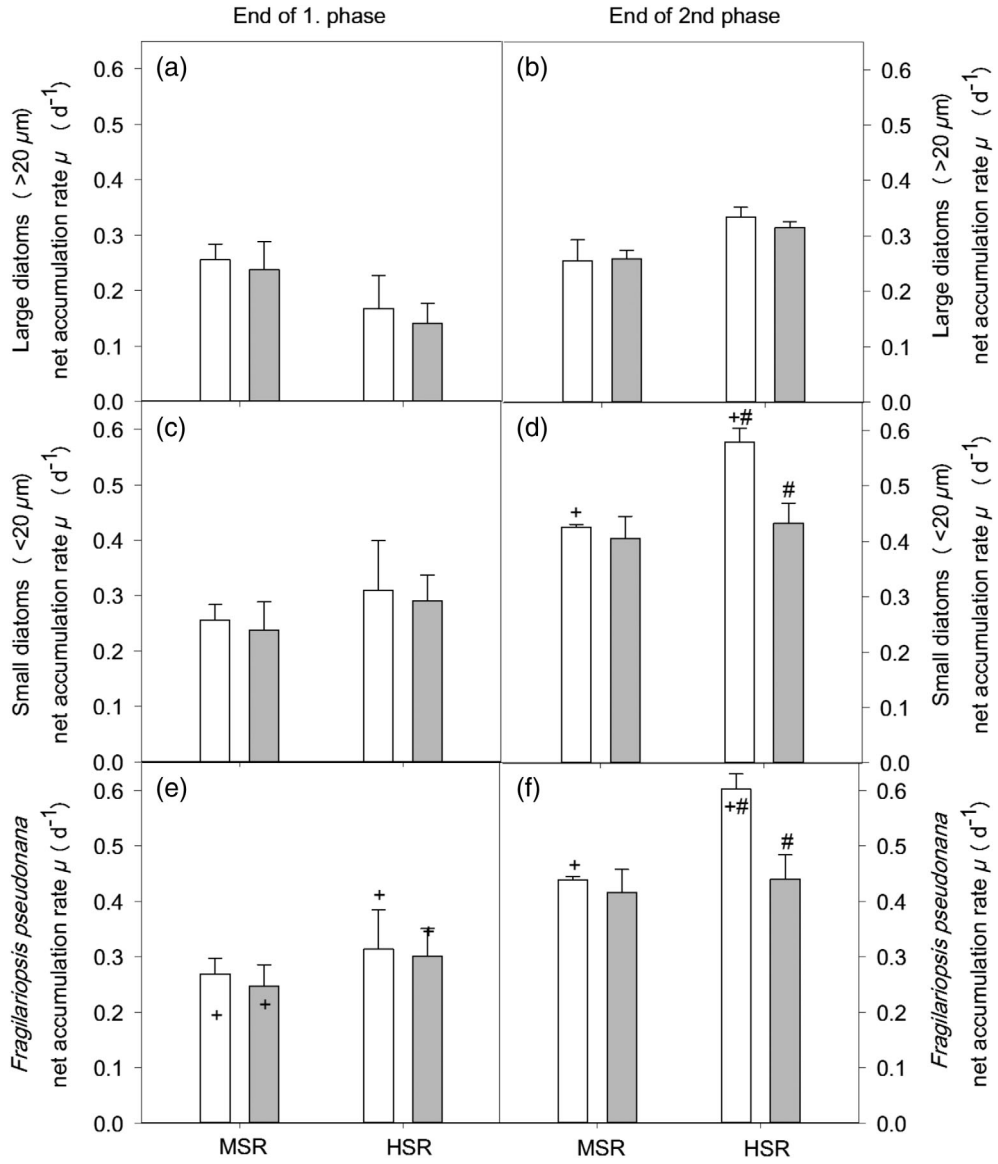

Fig. 4. Net accumulation rates (μ, d^{-1}) of the large (>20 μm; **a**, **b**) and the small (<20 μm; **c**, **d**) size diatom fraction as well as of the diatom *F. pseudonana* (**e**, **f**) determined after the first (**a**, **c**, **e**) and the second (**b**, **d**, **f**) experimental phase after exposure to MSR and HSR in combination with low, ambient, and high pCO_2. Values represent the means ($\pm$ SD) of triplicate incubations. Significant differences ($p < 0.05$) between treatments are indicated by + for light effects and # for pCO_2 effects.

pCO_2 (Fig. 4b). For this diatom size class, increasing pCO_2 had no effect on accumulation rates. The small-sized diatoms (post hoc: $p < 0.001$) and *F. pseudonana* (post hoc: $p < 0.001$) exhibited a light-dependent stimulation in accumulation rates at ambient, but not at high pCO_2 at the end of the experiment (Fig. 4d,f). The combination of HSR and elevated pCO_2 synergistically reduced accumulation rates of small-sized diatoms (two-way ANOVA: $p = 0.0067$) such as *F. pseudonana* (two-way ANOVA: $p = 0.0056$). The same trend was also found for the small diatom *F. curta* (data not shown).

At the end of the both experimental phases, accumulation rates of single-celled and colonial *P. antarctica* were neither altered by increasing solar radiation nor by changes in pCO_2 (Fig. 5). In comparison, irrespective of the experimental treatments accumulation rates of the colonial *P. antarctica* cells determined at the end of the first experimental phase were higher compared to those estimated at the end of the experiment (Fig. 5c,d).

Chl a fluorescence

Chl *a* fluorescence measurements gave a maximum photochemical yield (F_v/F_m) of 0.43 $\pm$ 0.02 in the start community (Table 3). After the end of the first experimental phase, increasing solar radiation reduced F_v/F_m values in all pCO_2 treatments (two-way ANOVA: $p < 0.0001$, Table 3). During this phase, increasing pCO_2 did not change F_v/F_m values in all

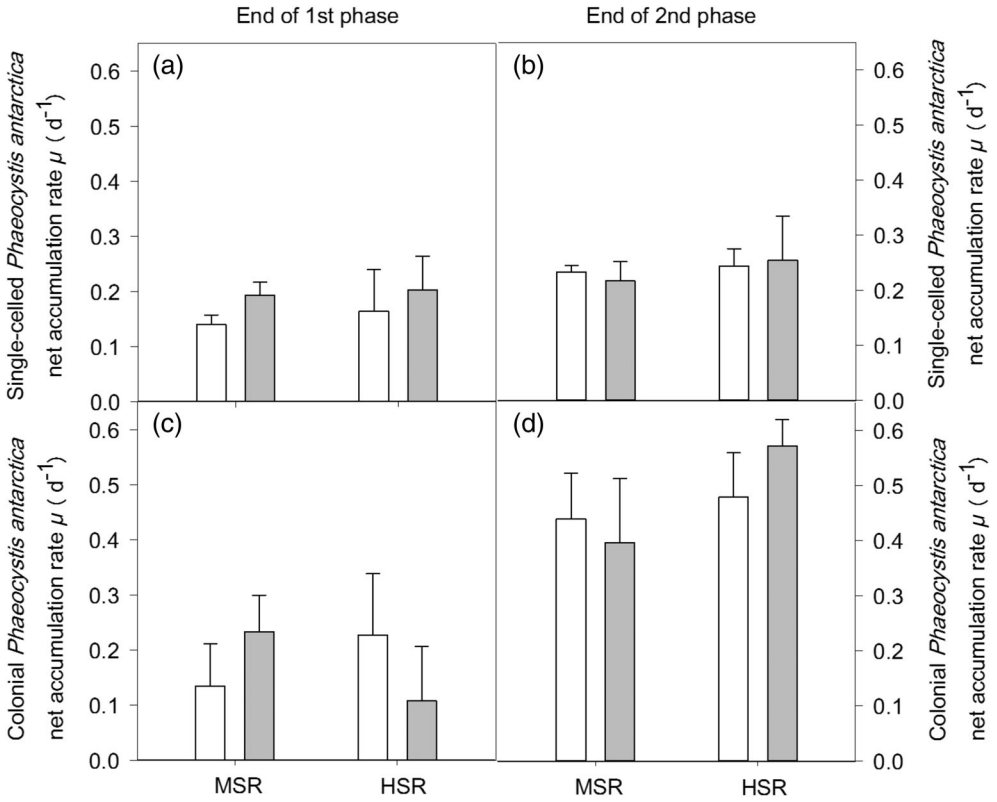

Fig. 5. Net accumulation rates (μ, d^{-1}) of single-celled (**a**, **c**) and colonial (**b**, **d**) *P. antarctica* determined after the first (**a**, **c**) and the second (**b**, **d**) experimental phase after exposure to MSR and HSR in combination with low, ambient, and high pCO_2. Values represent the means ($\pm$ SD) of triplicate incubations. Significant differences ($p < 0.05$) between treatments are indicated by + for light effects and # for pCO_2 effects.

light treatments. At the end of the experiment, F_v/F_m values were significantly reduced by 20% from MSR to HSR in the low pCO_2 treatments (post hoc: $p < 0.01$), but remained unaltered in the ambient and high pCO_2 treatments. Increasing pCO_2 did generally not affect final F_v/F_m values. Only at HSR, F_v/F_m values were enhanced by 32% from low to ambient pCO_2 (post hoc: $p < 0.01$), but declined by 16% from ambient to high pCO_2 (post hoc: $p < 0.05$).

Maximum electron transport rate (ETR_m) accounted for 371 ± 52 e^- $PSII^{-1}$ s^{-1} in the initially sampled phytoplankton community (Table 3). At the end of the first experimental phase, ETR_m significantly increased from MSR to HSR in all pCO_2 treatments (two-way ANOVA: $p < 0.0001$, Table 3). During this phase, pCO_2 did not influence ETR_m. At the end of the experiment, a light-dependent increase by 86% (post hoc: $p < 0.01$) and 65% (post hoc: $p < 0.05$) was observed in the low and high pCO_2 treatments, respectively, while no effect was found in the ambient pCO_2 treatment. Increasing pCO_2 had generally no effect on ETR_m except for the HSR treatments, which showed a decline in ETR_m by 36% (post hoc: $p < 0.05$) between low and ambient pCO_2.

Initially, the light saturation point of photosynthesis was reached at 134 ± 12 μmol photons m^{-2} s^{-1} (I_K, Table 3). After the first experimental phase, I_K remained unaffected between MSR and HSR at low pCO_2, but increased by 69% (post hoc: $p < 0.001$) and 140% (post hoc: $p < 0.0001$) at ambient and high pCO_2, respectively. During this phase, I_K remained generally constant irrespective of changes in pCO_2 except for the HSR treatment, where I_k values significantly differed between low and high pCO_2 (post hoc: $p < 0.01$). At the end of the experiment, no differences in I_K between pCO_2 and solar radiation treatments were observed.

The light use efficiency (α) was initially 2.80 ± 0.54 (Table 3). After the first experimental phase, α values did not change with increasing solar radiation in the ambient and high pCO_2 treatments whereas there was a light-dependent increase by 53% (post hoc: $p < 0.01$) in the low pCO_2 treatments. Increasing pCO_2 generally did not affect α apart from the HSR treatment, where α declined by 36% (post hoc: $p < 0.05$) between low and ambient pCO_2. Final α values were constant among the different light and pCO_2 treatments.

Initially, the functional absorption cross section of PSII (σ_{PSII}) accounted for 4.5 ± 0.3 nm^2 $PSII^{-1}$ (Table 3). During both experimental phases, σ_{PSII} was not affected by the two applied solar radiation treatments. The only exception was the low pCO_2 treatment, for which at the end of the first experimental phase σ_{PSII} was significantly enhanced by 44% from MSR to HSR (post hoc: $p < 0.01$). In response to increasing

Table 3. Maximum quantum yield of PSII photochemistry (F_v/F_m), maximum electron transport rates (ETR_m), light saturation point (I_K), light use efficiency (α), functional absorption cross section of PSIIs (σ_{PSII}), time constant for electron transfer at PSII (τ_{Qa}), and connectivity between adjacent photosystems (P) measured at the start and after two experimental phases in a natural phytoplankton community exposed to MSR and HSR, respectively in combination with low, ambient, and high pCO_2. Values represent the means (± SD) of triplicate incubations. Significant differences ($p < 0.05$) between treatments are indicated by + for light effects and # for pCO_2 effects.

Light treatment	pCO_2 treatment	F_v/F_m (rel. unit)	ETR_m ($e^- PSII^{-1} s^{-1}$)	I_K (μmol photons $m^{-2} s^{-1}$)	α (rel. unit)	σ_{PSII} ($nm^2 PSII^{-1}$)	P (rel. unit)	τ_{Qa} (μs)
Start		0.38 ± 0.05	371 ± 52	134 ± 12	2.80 ± 0.54	4.5 ± 0.3	0.31 ± 0.08	613 ± 48
End of first experimental phase:								
MSR	Low pCO_2	0.45 ± 0.04$^+$	300 ± 25$^+$	90 ± 4	3.33 ± 0.15$^+$	4.3 ± 0.3$^+$	0.29 ± 0.07	673 ± 21$^+$
	Ambient pCO_2	0.46 ± 0.02$^+$	250 ± 50$^+$	74 ± 16$^+$	3.40 ± 0.09	4.4 ± 0.1	0.30 ± 0.03	697 ± 8$^+$
	High pCO_2	0.44 ± 0.03$^+$	275 ± 29$^+$	83 ± 10$^+$	3.30 ± 0.06	5.3 ± 1.2	0.28 ± 0.04	673 ± 2
HSR	Low pCO_2	0.36 ± 0.03$^+$	524 ± 60$^+$	103 ± 9$^\#$	5.11 ± 0.57$^{+\#}$	6.2 ± 0.4$^+$	0.27 ± 0.05	607 ± 22$^+$
	Ambient pCO_2	0.37 ± 0.03$^+$	401 ± 81$^+$	125 ± 14$^+$	3.26 ± 0.88$^\#$	4.9 ± 0.7	0.25 ± 0.03	643 ± 26$^+$
	High pCO_2	0.36 ± 0.03$^+$	501 ± 57$^+$	146 ± 0$^{+\#}$	3.27 ± 0.40	4.7 ± 0.3	0.21 ± 0.06	671 ± 11
End of second experimental phase:								
MSR	Low pCO_2	0.45 ± 0.04$^+$	673 ± 210$^+$	188 ± 51	3.64 ± 1.01	6.5 ± 0.5	0.28 ± 0.01$^+$	552 ± 44
	Ambient pCO_2	0.43 ± 0.02	503 ± 146	175 ± 114	3.30 ± 1.31	6.3 ± 1.4	0.23 ± 0.03	583 ± 76
	High pCO_2	0.41 ± 0.02	601 ± 77$^+$	184 ± 12	3.26 ± 0.21	5.9 ± 0.3	0.21 ± 0.02	552 ± 9
HSR	Low pCO_2	0.34 ± 0.05$^{+\#}$	1249 ± 232$^{+\#}$	359 ± 119	3.62 ± 0.69	6.3 ± 0.6	0.18 ± 0.05$^+$	531 ± 6
	Ambient pCO_2	0.45 ± 0.02$^\#$	805 ± 181$^\#$	253 ± 89	3.29 ± 0.49	5.7 ± 1.1	0.23 ± 0.04	600 ± 56
	High pCO_2	0.38 ± 0.01$^\#$	993 ± 18$^+$	372 ± 140	2.77 ± 0.75	5.8 ± 0.8	0.21 ± 0.00	584 ± 63

pCO_2, σ_{PSII} also remained unchanged at the end of both experimental phases.

The connectivity of adjacent PSIIs (***p***, Table 3) accounted for 0.31 ± 0.08 at the start of the experiment and generally remained unaffected by the applied solar radiation regimes after both experimental phases. Only at the end of the experiment, ***p*** declined by 36% from MSR to HSR in the low pCO_2 treatments (post hoc: $p < 0.01$). At the end of both experimental phases, ***p*** did not change with increasing pCO_2 under both light conditions.

Initially, the time constant for electron transfer at PSII (τ_{Qa}) reached 613 ± 48 μs (Table 3). At the end of the first phase, τ_{Qa} declined from MSR to HSR by 10% (post hoc: $p < 0.01$) and 8% (post hoc: $p < 0.05$) in the low and ambient pCO_2 treatments, respectively, but did not change in the high pCO_2 treatment. After the second experimental phase, increasing solar radiation had no effect on τ_{Qa} in all pCO_2 treatments. After both experimental phases, τ_{Qa} was not altered by increasing pCO_2.

Discussion

Due to the importance of the coastal SO in sequestering anthropogenic CO_2 (Arrigo et al. 2008), understanding the effects of increasing natural solar radiation regimes under different CO_2 scenarios on SO primary productivity and phytoplankton species composition can help to elucidate their combined effects on the biological carbon pump in the present and future ocean. As the WAP is an important region in overall productivity, we chose the RaTS 1 site in Ryder Bay as a sampling location, which is one of the longest running year-round oceanographic monitoring stations in coastal Antarctica (Clarke et al. 2008). From this site, the phytoplankton community was collected in mid-February 2015 and was numerically dominated by single-celled *P. antarctica* (1721 ± 82 cells mL^{-1}, 52% ± 2%, Fig. 3). Based on cell count data, diatoms contributed to 7% ± 1% of the whole community (219 ± 24 cells mL^{-1}, Fig. 3), with the small pennate species *F. pseudonana* being predominant (91 ± 3 cells mL^{-1}, Fig. 3). Even though *P. antarctica* may dominate in terms of cell abundance, it, however, has a comparably small C content (13.6 pg C $cell^{-1}$, Annett et al. 2010) relative to the less abundant large diatom species such as *O.* cf. *weissflogii* (30 ± 6 cells mL^{-1}), *E.* cf. *antarctica* (11 ± 4 cells mL^{-1}), *Navicula* sp. (3 ± 1 cells mL^{-1}), *Pseudo-nitzschia* sp. (12 ± 3 cells mL^{-1}), and *T.* cf. *antarctica* (4 ± 2 cells mL^{-1}) with a high C content (2318 pg C $cell^{-1}$, 1767 pg C $cell^{-1}$, 162 pg C $cell^{-1}$, 147 pg C $cell^{-1}$, and 1677 pg C $cell^{-1}$, respectively, Annett et al. 2010). Our seawater sampling from surface waters at the RaTS 1 site took place during a day under a solar radiation of 130 μmol photons m^{-2} s^{-1}. Accordingly, the light saturation point of photosynthesis was reached at 134 ± 12 μmol photons m^{-2} s^{-1} (I_K, Table 3). As typical for late summer for coastal waters of this region (Garibotti et al. 2005; Trimborn et al. 2015; Young et al. 2015; Rozema et al. 2017*a*), biomass of the sampled community was moderate (Chl *a*: 3.5 μg L^{-1} and POC: 394 μg L^{-1}). Based on the seawater column Chl *a* concentrations estimated at the RaTS site in the framework of the long-term monitoring program, our sampling took place at a late stage of the phytoplankton bloom. In line with this, concentrations of nitrate (5.14 μM) and nitrite (0.07 μM) as well as pCO_2 (181 μatm) were low in our sampled seawater while concentrations of phosphate (0.64 μM) and silicate (45 μM) were high. Similar concentrations were previously reported during late summer blooms in Ryder Bay (Annett et al. 2010; Clarke et al. 2008; Henley et al. 2017; Jones et al. 2017; Rozema et al. 2017*b*). Long-term data collection further demonstrates that transient nitrogen limitation is commonly observed at the RaTS site at this time of the year, while concentrations of phosphate and silicate are not usually depleted (Clarke et al. 2008; Henley et al. 2017). In this study, as nitrate was not initially limiting in each phase of our experiment (~5 μM), we argue that phytoplankton was exposed to transient nitrate drawdown, as observed by the high C : N ratios in all incubations at the end of both experimental phases (~7–12 mol mol^{-1}, Table 2). Similarly, nitrate limitation increased C : N ratios in a laboratory experiment with the diatom *Phaeodactylum tricornutum* irrespective of whether it was grown at 390 μatm or 1000 μatm pCO_2 (7 mol mol^{-1} or 9 mol mol^{-1}, respectively, Li et al. 2012). Even higher C : N ratios were estimated in response to nitrate drawdown in a coastal phytoplankton community of East Antarctica, reaching 12 mol mol^{-1} and 15 mol mol^{-1} at 643 μatm and 1281 μatm pCO_2, respectively (Davidson et al. 2016). At the same location, elevated C : N ratios (7 up to 12 mol mol^{-1}) were also observed across a range of various pCO_2 levels (343 up to 1641 μatm) at the end of another minicosm experiment (Deppeler et al. 2018). The high C : N ratios determined in our study resulted from higher mean POC contents (1367.0 ± 263.3 μmol L^{-1} and 1020.1 ± 186.2 μmol L^{-1}) relative to the constant low mean PON contents (170.2 ± 8.9 μmol L^{-1} and 111.8 ± 22.8 μmol L^{-1}) determined at the end of the first and the second phase, respectively. Such carbon overconsumption (Banse 1994; Toggweiler 1994) was previously reported for diatom-dominated phytoplankton communities under nitrate limitation (Engel et al. 2002; Taucher et al. 2012). In accord with this, nitrate limitation did not affect carbon buildup or PP of a *Phaeocystis pouchetii* dominated bloom in Belgian coastal waters (Lancelot and Mathot 1987), Arctic (Kulk et al. 2018; van de Poll et al. 2018) and Antarctic coastal phytoplankton assemblages (Davidson et al. 2016; Deppeler et al. 2018). Superimposed on transient nitrogen drawdown at the end of each experimental phase, we also observed significant effects by increasing solar radiation and pCO_2 that will be discussed in the following.

1. Phase: Increasing solar radiation reduced PP and enhanced light protection

As previously observed for the Marguerite Bay area (Garibotti et al. 2003, 2005) including Ryder Bay (Clarke et al. 2008), large phytoplankton cells (>20 μm) were the primary contributors to PP with 65% (0.24 ± 0.05 μmol C [μmol POC]$^{-1}$ h^{-1}) in the initial phytoplankton community whereas small cells (<20 μm) contributed to a lower degree (35%, 0.13 ± 0.02 μmol C [μmol POC]$^{-1}$ h^{-1}). Compared to the start of the experiment, exposure

to MSR promoted stimulation in PP of the large, but not of the small, phytoplankton fraction in all pCO_2 treatments at the end of the first experimental phase (Fig. 2c,e). Based on photophysiological characteristics such as ETR_m and I_k (Table 3), the initial phytoplankton community resembled more the photoacclimation characteristics of the HSR than of the MSR treatments. In fact, average daily irradiances of the initial community (130 μmol photons m^{-2} s^{-1}) and the HSR treatments (260 $\pm$ 43 μmol photons m^{-2} s^{-1}) were similar, but higher compared to the MSR treatments (82 $\pm$ 24 μmol photons m^{-2} s^{-1}) (Fig. 1). Accordingly, F_v/F_m values were slightly higher for all MSR treatments (0.44–0.46) compared to the initial value of 0.38 $\pm$ 0.05 (Table 3), even though this effect was not statistically significant. Nonetheless, it is perhaps suggestive that the overall stimulation in PP of the large phytoplankton size class among all MSR treatments hints at relief of high light stress relative to the start of the experiment. Surprisingly, the low pCO_2 treatment displayed the strongest stimulation at MSR, with a doubling of PP for the large size class (Fig. 2c). In comparison, the ambient and high pCO_2 treatments also showed stimulation in PP, but to a lower extent (Fig. 2c). As the initially sampled phytoplankton community was actually grown under the same pCO_2 as before sampling (Table 1, 181 μatm), it could be that the stimulation in PP of the large size class was potentially dampened in the ambient and high pCO_2 treatments as cells still needed in addition to the MSR conditions also to acclimate to the higher pCO_2 levels. In support of this, large phytoplankton in particular were previously found to be better adapted to cope with variable pH conditions compared with small-sized cells (Flynn et al. 2012; Thoisen et al. 2015). It needs to be noted that C : N ratios were enhanced in all MSR treatments relative to the start community, but did not display any CO_2-dependent changes (Table 2). Considering also that nitrate limitation did not affect carbon buildup in previous studies (Lancelot and Mathot 1987; Davidson et al. 2016; Deppeler et al. 2018; Kulk et al. 2018; van de Poll et al. 2018), we suggest that transient nitrate drawdown did not negatively influence PP. Such changes in productivity did further not translate into changes in species composition, as the latter was similar between the start and the end of the first experimental phase (Fig. 3). Hence, irrespective of the applied pCO_2, as for the start, all MSR communities were still numerically dominated by single celled *P. antarctica* (~60–70%, Fig. 3), a species that was already found to be tolerant to a broad range of pCO_2 and light levels (Moisan and Mitchell 1999; Arrigo et al. 2010; Hoogstraten et al. 2012*a*; Trimborn et al. 2013, 2017*a*,*b*; Thoisen et al. 2015; Koch et al. 2019). Despite the presence of *P. antarctica* in the initial community of previous bottle incubation experiments, elevated pCO_2 in many cases did not stimulate its relative abundance (Tortell et al. 2008; Feng et al. 2010; Hoppe et al. 2013; Young et al. 2015). Only Trimborn et al. (2017*b*) reported an OA-dependent shift from an initially diatom-dominated phytoplankton community toward a dominance of solitary celled *P. antarctica* at low and high iron availability. In this study, irrespective of the pCO_2 an overall increase in the abundance of the diatom *F. pseudonana* among the diatom population was observed in all MSR treatments after the first experimental phase (Fig. 3). Accordingly, there was no change in its accumulation rate among the different treatments (Fig. 4e). Our results are in agreement with previous observations for *F. curta* (Coad et al. 2016; Heiden et al. 2016; Trimborn et al. 2017*b*), *Fragilariopsis cylindrus* (Coad et al. 2016) *F. kerguelensis* (Trimborn et al. 2017*a*), or small-sized *Fragilariopsis* spp. (<20 μm, Hancock et al. 2018), but are opposed to the OA-dependent stimulation in abundance of *F. cylindrus* (Hoppe et al. 2013) or *F. curta*/*cylindrus* (Davidson et al. 2016). Based on the different observations, inter- and intraspecific differences in the CO_2 sensitivity appear to exist among the genus *Fragilariopsis*, which were potentially further modulated by the different applied light regimes.

Between MSR and HSR, species composition also remained unaffected at the end of the first experimental phase (Fig. 3). In line with this, net accumulation rates of small- and large-sized diatoms including *F. pseudonana* as well as of the single-celled and colonial *P. antarctica* were constant (Figs. 4a,c,e, 5a,c). Even though species composition did not change, a higher photosensitivity of all HSR relative to the MSR treatments was shown by the significantly reduced F_v/F_m values (Table 3). Even though the daily irradiance accounted on average for 260 $\pm$ 43 μmol photons m^{-2} s^{-1}, light saturation of photosynthesis was already reached between 103 μmol photons m^{-2} s^{-1} and 146 μmol photons m^{-2} s^{-1} depending on the pCO_2 level (Table 3). Together with the strongly enhanced ETR_m across the tested pCO_2 levels (Table 3), these findings point toward the saturation of the Calvin cycle and thus the requirement for alternative electron cycling to dissipate excessive light energy. In support of this, communities shifted from light-harvesting to photoprotection between MSR and HSR, as indicated by the increased ratio of light protective pigments relative to Chl *a* (diadino- and diatoxanthin:Chl *a*) and the lowered Chl *a* : POC ratios in all pCO_2 treatments (Table 2). Similar light-dependent photoacclimation was previously observed in natural Antarctic phytoplankton assemblages in response to high irradiance (Feng et al. 2010; van de Poll et al. 2011; Alderkamp et al. 2013). At the expense of carbon fixation, high cyclic electron transport around PSI represents an important strategy to prevent overexcitation of PSII in particular under high irradiance (Heber et al. 1978; Falk and Palmqvist 1992). Such photoprotective process was previously found to be active under high irradiance in Antarctic phytoplankton (Alderkamp et al. 2012) and could explain the here overall lowered productivity of the whole phytoplankton community of the HSR (0.26–0.30 μmol C [μmol POC]$^{-1}$ h^{-1}) relative to the MSR treatments (0.50–0.75 μmol C [μmol POC]$^{-1}$ h^{-1}). In fact, this trend was mainly driven by the significant decline in PP rates of the large, and not of the small, phytoplankton size fraction (Fig. 2a,c,e). Even though the negative high light effect was not reflected in species composition (Fig. 3), it is interesting to note that small-sized phytoplankton became more important contributors to PP with ~40% in all HSR treatments while they only accounted for ~20% up to 30% depending on the pCO_2 level at MSR (Fig. 2a,c,e). Interestingly, the strongest sensitivity toward high light was observed in the low pCO_2 treatment, where PP of the large size

class declined by 75% (Fig. 2c). For this treatment, surprisingly α and σ_{PSII} were significantly enhanced from MSR to HSR while τ_{Qa} decreased (Table 3), suggesting a higher light-use efficiency. This effect was, however, not translated into higher productivity, but dissipated as excess light energy (Table 2). In line with this, a laboratory study revealed that the combination of low pCO_2 and various light levels was especially stressful in terms of growth and carbon buildup for the large-sized *O. weissflogii* compared with the small-sized *F. curta* (Heiden et al. 2016).

OA, particularly in combination with high irradiance, was found to amplify the negative effects on growth and/or carbon fixation and caused higher photosensitivity of Antarctic diatoms in various laboratory experiments (Hoogstraten et al. 2012*b*; Hoppe et al. 2015; Heiden et al. 2016, 2018; Trimborn et al. 2017*a*). In this study, all tested parameters remained unaffected in response to elevated pCO_2 and HSR after the first experimental phase (Tables 2–3; Figs. 2–5). Only C : N ratios showed a significant rise between ambient and high pCO_2 (Table 2). Contrary to this, in previous OA studies with Antarctic coastal phytoplankton assemblages when nitrate was exhausted C : N ratios were found to be highest in the low pCO_2 treatments (Davidson et al. 2016; Deppeler et al. 2018). The latter studies also showed that these high C : N ratios were primarily the result of nitrate depletion and not CO_2 availability. As the highest C : N ratio was observed here in the high pCO_2 treatment at HSR, this suggests that these communities could have experienced the highest nitrate stress relative to the other treatments. Hence, it cannot be ruled out completely that the observed negative light effect on PP of the large phytoplankton fraction was amplified by transient nitrate exhaustion, in particular in the OA treatment, at the end of the first growth phase. Considering, however, also that all other measured physiological parameters remained constant under these conditions (Tables 2–3; Figs. 3–5), this somewhat argues against nitrate depletion as strong control on phytoplankton physiology. As transient nutrient stress in combination with changes in light and pCO_2 availability occur frequently in Ryder Bay during late summer (Annett et al. 2010; Clarke et al. 2008; Henley et al. 2017; Jones et al. 2017; Rozema et al. 2017*b*), our results instead show that all HSR communities were well adapted to cope with such environmental conditions.

2. Phase: OA and HSR together reduced cell abundances of *F. pseudonana*, but not of *P. antarctica*

During the second experimental phase, mean daily irradiances reached on average 141 ± 48 μmol photons m^{-2} s^{-1} d^{-1} and 508 ± 190 μmol photons m^{-2} s^{-1} d^{-1} in the MSR and HSR treatments, respectively (Fig. 1). In comparison with the first phase, mean daily irradiances were twice as high (Fig. 1). Adjustment of all communities (MSR and HSR) to the higher light regimes was apparent, as light saturation characteristics such as I_k and ETR_m doubled while α remained the same as before (Table 3). Only after the first phase, the MSR communities displayed lowered Chl *a* : POC ratios, reaching therewith similar low ratios as the HSR communities (Table 2). Despite much higher daily mean irradiances during the second phase, productivity of the whole community was similarly high in all treatments, ranging between 0.33 μmol C (μmol POC)$^{-1}$ h^{-1} and 0.44 μmol C (μmol POC)$^{-1}$ h^{-1} (Fig. 2b). In contrast to the first phase, at the end of the experiment, small phytoplankton became the primary contributors to PP, accounting for 0.23 up to 0.33 μmol C (μmol POC)$^{-1}$ h^{-1} (61–85%, Fig. 2d,f). Moreover, no CO_2-dependent changes in productivity or phytoplankton physiology (except for F_v/F_m at HSR) were found for all treatments, indicating a high acclimation capacity of all assemblages despite higher light availability over the second phase. Similarly, no differences in species composition and photophysiology (F_v/F_m, ETR_m) across a range of increasing pCO_2 levels were evident at the end of several OA bottle incubation experiments, explained by an acclimation of the present community to the experimental conditions (Coad et al. 2016). Such high acclimation capacity across a range of different pCO_2 levels is not surprising due to the wide range of pH fluctuations naturally occurring in coastal WAP waters such as Ryder Bay (Jones et al. 2017).

The final phytoplankton species composition was generally not affected by the applied changes in light and CO_2 availability apart from the HSR treatment grown at ambient pCO_2. Except for the latter treatment, final phytoplankton communities were still numerically dominated by *P. antarctica* (46–62%). Whereas over the first phase solitary cells were most abundant, at the end of the experiment, half of the cells were in the colonial form (Fig. 3). Opposed to solitary *P. antarctica* cells, which showed similar high accumulation rates among all treatments (Fig. 5b), the higher abundance of colonial *P. antarctica* resulted from its much higher accumulation over the second phase (Fig. 5d). Higher growth by colonial than solitary cells was previously reported for *P. antarctica* (Shields and Smith 2009) and *Phaeocystis globosa* (Wang et al. 2011). Considering further that nutrient limitation (nitrate, phosphate, and iron) was found to enhance the cell abundance of solitary *Phaeocystis* cells, the increased number of colonial cells observed over the second phase suggests that transient nitrate exhaustion did not influence its accumulation (Veldhuis and Admiraal 1987; Peperzak 1993; Riegman and von Boekel 1996; Verity et al. 2007; Bender et al. 2018). Moreover, colonial *P. globosa* cells were more effective competitors under high light conditions due to mucus formation, which was suggested to act as an energy drain mechanism storing fixed carbon in the form of polysaccharides inside the mucoid matrix (Riegman and von Boekel 1996). In line with this, colony formation of *P. antarctica* within a natural phytoplankton assemblage of the Ross Sea was favored under a high (52–276 μmol photons m^{-2} s^{-1}) relative to a low natural light regime (11–58 μmol photons m^{-2} s^{-1}, Feng et al. 2010). Based on our results, cell abundance of solitary relative to colonial cells as well as the number of colonies of the *P. antarctica* strain of

Ryder Bay was similar between MSR and HSR treatments at the end of the experiment (Fig. 3), pointing toward a high light tolerance also of the single-celled *P. antarctica*. Similar findings were previously made for a single celled strain when exposing it to increasing irradiances (Trimborn et al. 2017*a*).

Between the first and second experimental phase, the overall contribution of diatoms relative to the other counted phytoplankton species increased, accounting for 27 up to 59%, Fig. 3). The latter response was mainly driven by enhanced accumulation of small diatoms before and after dilution (Fig. 4b,d). A general trend toward smaller-celled communities with increased pCO_2 was already reported in OA studies globally (Schulz et al. 2017), but also for small-sized (<20 μm) Antarctic diatoms (Trimborn et al. 2017*b*; Deppeler et al. 2018; Hancock et al. 2018). In line with this, the increased cell abundance of small diatoms here resulted from enhanced accumulation rates of the small *F. pseudonana* (Fig. 4f), being therefore the most abundant species among diatoms in all treatments (Fig. 3). Even though small diatoms became generally more abundant over the second experimental phase, final phytoplankton communities were still numerically dominated by *P. antarctica* (46–62%, Fig. 3). Surprisingly, only the communities grown under ambient pCO_2 in conjunction with HSR were dominated by diatoms (66% $\pm$ 15%, Fig. 3), in particular *F. pseudonana* (59% $\pm$ 11%, Fig. 3). Congruently, accumulation rates of small diatoms such as *F. pseudonana* were significantly stimulated between MSR and HSR when grown at ambient pCO_2 (Fig. 4d,f). Such trend in response to HSR was, however, absent at high pCO_2. Hence, the combination of high pCO_2 and HSR together synergistically reduced the abundances of small diatoms such as *F. pseudonana*. In line with this, growth and POC production of *F. curta* were negatively affected when grown at 200 μmol photons m^{-2} s^{-1} combined with 1000 μatm pCO_2 (Heiden et al. 2016). Next to the light-dependent stimulation in cell abundances of small diatoms such as *F. pseudonana*, photochemical efficiencies remained unaltered between MSR and HSR at ambient pCO_2, but were reduced at high pCO_2 (Table 3). Hence, this negative effect was related to the higher photosensitivity of the phytoplankton community when grown at HSR in conjunction with high pCO_2. Similar findings were previously observed under such conditions for a mixed phytoplankton community from the Ross Sea (Feng et al. 2010) as well as various Antarctic diatoms in laboratory experiments (Hoppe et al. 2015; Heiden et al. 2016; Trimborn et al. 2017*a*; Heiden et al. 2018). In comparison, such negative growth responses were not found for *P. antarctica* (Trimborn et al. 2013, 2017*a*,*b*; Thoisen et al. 2015; Koch et al. 2019). In particular, the colonial form of *P. antarctica* was found to exhibit a better ability to cope with variable CO_2 conditions as they themselves generate these over the light : dark cycle (Flynn et al. 2012).

Next to *P. antarctica* and diatoms, based on microscopic counts, other flagellate species accounted for 7–11% within the different communities at the end of the experiment (Fig. 3). After dilution, the overall contribution of other flagellate species was even lower in all treatments, indicating no specific treatment related response. Similar observations for flagellates were previously made in a CO_2-Fe incubation experiment with a natural phytoplankton assemblage from the Weddell Sea (Hoppe et al. 2013). Unfortunately, no information yet exists on the CO_2 sensitivity of taxon groups such as Antarctic cryptophytes, prasinophytes, and dinoflagellates. As cryptophytes are expected to become more abundant in coastal WAP waters as a result of rising temperatures and ice melting (Moline et al. 2004; Montes-Hugo et al. 2009), future studies should also consider this phytoplankton group in their experimental OA studies.

Implications for PP and species composition of Ryder Bay in the future

This study shows that overall primary productivity of Ryder Bay phytoplankton was insensitive in response to the changes in light and CO_2 availability as projected for the future coastal SO. In agreement with results from Antarctic phytoplankton assemblages from other regions of the coastal SO (Davidson et al. 2016; Deppeler et al. 2018; Hancock et al. 2018), the coastal phytoplankton assemblage tested here displayed a high acclimation capacity of its physiology over the first experimental phase. Even though counteracted by adjustments in photoprotection, the observed higher photosensitivity between MSR and HSR resulted in lowered PP rates of the whole community and especially of large phytoplankton at the end of the first experimental phase. In contrast to previous findings (Hoogstraten et al. 2012*a*,*b*; Hoppe et al. 2015; Heiden et al. 2016, 2018; Trimborn et al. 2017*a*), such negative light effect on PP was not amplified by increasing pCO_2 levels, but instead showed the opposite trend. As expected for the coastal environment, which is exposed to seasonal fluctuations in pCO_2, light availability and nutrients (Annett et al. 2010; Henley et al. 2017; Jones et al. 2017; Rozema et al. 2017*b*), after the first experimental phase the phytoplankton community had adjusted to these conditions. As a consequence, PP at the end of the experiment yielded similar high rates as at the start of the experiment, but with the main contributors shifting from initially large to small cells toward the end. This response was mainly the result of an overall enhanced cell abundance of the small diatom *F. pseudonana* among all treatments. Interestingly, while final communities were still numerically dominated by *P. antarctica* among most treatments, we also found a significant high light-dependent stimulation in cell abundance of *F. pseudonana*, but only at ambient pCO_2. Due to the higher photosensitivity of the latter when exposed to the combined effects of HSR and OA, this positive effect was, however, alleviated thus counteracting its competitive advantage. As the two dominant groups that form large phytoplankton blooms in Antarctic coastal waters are diatoms and *P. antarctica* (DiTullio and Smith 1996; Arrigo et al. 2000; Smith and Asper 2001; Garibotti et al. 2003; Annett et al. 2010), in agreement with previous studies (Hoogstraten

et al. 2012*a*; Trimborn et al. 2013, 2017*a*; Thoisen et al. 2015; Koch et al. 2019), this study further strengthens future projections that *P. antarctica* might increase its competitiveness toward diatoms under OA irrespective of light availability. *P. antarctica* was reportedly found in high abundances early in spring (DiTullio and Smith 1996; DiTullio et al. 2000; Smith and Asper 2001) with deep mixed layer depths and thus high pCO_2 levels and low daily irradiances, pointing toward its better ability to adjust its photosynthetic efficiency (Palmisano et al. 1986; Arrigo et al. 1999; Moisan and Mitchell 1999). In line with the conclusion of Feng et al. (2010), our study further underlines that the relative abundance of *P. antarctica* during the season is not necessarily linked to its photobiology and an increase in daily integrated irradiances, but more to its overall high tolerance to a broad range of pCO_2 and light levels. This also matches the findings of Rozema et al. (2017*a*) that reported no correlation of haptophyte abundance to mixed layer depth in Ryder Bay. Even though primary productivity of Ryder Bay may remain unaltered, the observed shifts in PP from large toward small phytoplankton as main contributors can have a strong influence on whether this region will act as a source or sink of carbon in the future. This, however, will also strongly depend on its carbon export efficiency, with small cells considered to have a lower carbon export potential, thus potentially reducing the biological CO_2 sequestration potential of this region in the future.

References

Alderkamp, A.-C., G. Kulk, A. G. J. Buma, R. J. W. Visser, G. L. Van Dijken, M. M. Mills, and K. R. Arrigo. 2012. The effect of iron limitation on the photophysiology of *Phaeocystis antarctica* (Prymnesiophyceae) and *Fragilariopsis cylindrus* (Bacillariophyceae) under dynamic irradiance. J. Phycol. **48**: 45–59. doi:10.1111/j.1529-8817.2011.01098.x

Alderkamp, A.-C., M. M. Mills, G. L. Van Dijken, and K. R. Arrigo. 2013. Photoacclimation and non-photochemical quenching under in situ irradiance in natural phytoplankton assemblages from the Amundsen Sea, Antarctica. Mar. Ecol. Prog. Ser. **475**: 15–34. doi:10.3354/meps10097

Annett, A. L., D. S. Carson, X. Crosta, A. Clarke, and R. S. Ganeshram. 2010. Seasonal progression of diatom assemblages in surface waters of Ryder Bay, Antarctica. Polar Biol. **33**: 13–29. doi:10.1007/s00300-009-0681-7

Arrigo, K. R., D. H. Robinson, D.- L. Worthen, R. B. Dunbar, G. R. DiTullio, M. VanWoert, and M. P. Lizotte. 1999. Phytoplankton community structure and the drawdown of nutrients and CO_2 in the Southern Ocean. Science **283**: 365–367. doi:10.1126/science.283.5400.365

Arrigo, K. R., G. R. DiTullio, R. B. Dunbar, D. H. Robinson, M. VanWoert, D.- L. Worthen, and M. P. Lizotte. 2000. Phytoplankton taxonomic variability in nutrient utilization and primary production in the Ross Sea. J. Geophys. Res. **105**: 8827–8846. doi:10.1029/1998JC000289

Arrigo, K. R., G. van Dijken, and M. Long. 2008. Coastal Southern Ocean: A strong anthropogenic CO_2 sink. Geophys. Res. Lett. **35**: 1–6. doi:10.1029/2008GL035624

Arrigo, K. R., M. M. Mills, L. R. Kropuenske, G.- L. Van Dijken, A. C. Alderkamp, and D. H. Robinson. 2010. Photophysiology in two major southern ocean phytoplankton taxa: Photosynthesis and growth of *Phaeocystis antarctica* and *Fragilariopsis cylindrus* under different irradiance levels. Integr. Comp. Biol. **50**: 950–966. doi:10.1093/icb/icq021

Banse, K. 1994. Uptake of inorganic carbon and nitrate by marine plankton and the Redfield Ratio. Global Biogeochem. Cycles **4**: 81–84. doi:10.1029/93GB02865

Bender, S. J., D. M. Moran, M. R. McIlvin, H. Zheng, J. P. McCrow, J. Badger, G. R. DiTullio, A. E. Allen, and M. A. Saito. 2018. Iron triggers colony formation in *Phaeocystis antarctica*: Connecting molecular mechanisms with iron biogeochemistry. Biogeosci. **15**: 4923–4942. doi:10.5194/bg-2017-558

Boelen, P., W. H. van de Poll, H. J. van der Strate, I. A. Neven, J. Beardall, and A. G. J. Buma. 2011. Neither elevated nor reduced CO_2 affects the photophysiological performance of the marine Antarctic diatom *Chaetoceros brevis*. J. Exp. Mar. Biol. Ecol. **406**: 38–45. doi:10.1016/j.jembe.2011.06.012

Boyd, P. W., S. T. Lennartz, D. M. Glover, and S. C. Doney. 2015. Biological ramifications of climate-change-mediated oceanic multi-stressors. Nat. Clim. Chang. **5**: 71–79. doi:10.1038/nclimate2441

Clarke, A., M. P. Meredith, M. I. Wallace, M. A. Brandon, and D. N. Thomas. 2008. Seasonal and interannual variability in temperature, chlorophyll and macronutrients in northern Marguerite Bay, Antarctica. Deep-Sea Res. Part II Top. Stud. Oceanogr. **55**: 1988–2006. doi:10.1016/j.dsr2.2008.04.035

Coad, T., A. McMinn, D. Nomura, and A. Martin. 2016. Effect of elevated CO_2 concentration on microalgal communities in Antarctic pack ice. Deep-Sea Res. Part II Top. Stud. Oceanogr. **131**: 160–169. doi:10.1016/j.dsr2.2016.01.005

Davidson, A. T., J. McKinlay, K. Westwood, P. G. Thomson, R. van den Enden, M. de Salas, S. Wright, R. Johnson, and K. Berry. 2016. Enhanced CO_2 concentrations change the structure of Antarctic marine microbial communities. Mar. Ecol. Progr. Ser. **552**: 93–113. doi:10.3354/meps11742

Deppeler, S., K. Petrou, K. G. Schulz, K. Westwood, I. Pearce, J. McKinlay, and A. Davidson. 2018. Ocean acidification of a coastal Antarctic marine microbial community reveals a critical threshold for CO_2 tolerance in phytoplankton productivity. Biogeosciences **15**: 209–231. doi:10.5194/bg-15-209-2018

Dickson, A. G. 1981. An exact definition of total alkalinity and a procedure for the estimation of alkalinity and total inorganic carbon from titration data. Deep-Sea Res. Part A Oceanogr. Res. Pap. **28**: 609–623. doi:10.1016/0198-0149(81)90121-7

Dickson, A. G., and F. J. Millero. 1987. A comparison of the equilibrium constants for the dissociation of carbonic acid in

seawater media. Deep-Sea Res. Part A Oceanogr. Res. Pap. **34**: 1733–1743. doi:10.1016/0198-0149(87)90021-5

Dickson, A. G., C. L. Sabine, and J. R. Christian. 2007. Guide to best practices for ocean CO_2 measurements, p. 191. PICES Special Publication 3. Marine Science Organization.

DiTullio, G. R., and W. O. Smith. 1996. Spatial patterns in phytoplankton biomass and pigment distributions in the Ross Sea. J. Geophys. Res. **101**: 18467–18477. doi:10.1029/96JC00034

DiTullio, G. R., J. M. Grebmeier, K. R. Arrigo, M. P. Lizotte, D. H. Robinson, A. Leventer, J. P. Barry, M. L. VanWoert, and R. B. Dunbar. 2000. Rapid and early export of *Phaeocystis antarctica* blooms in the Ross Sea, Antarctica. Nature **404**: 595–598. doi:10.1038/35007061

Ducklow, H. W., K. Baker, D. G. Martinson, L. B. Quetin, R. M. Ross, R. C. Smith, S. E. Stammerjohn, M. Vernet, and W. Fraser. 2007. Marine pelagic ecosystems: The West Antarctic Peninsula. Philos Trans R. Soc. B Biol Sci **362**: 67–94. doi:10.1098/rstb.2006.1955

Edler, L. 1979. Recommendations for marine biological studies in the Baltic Sea: Phytoplankton and chlorophyll, p. 5–38. Baltic Mar. Biol. Public. 5. Department of Marine Botany, University of Lund.

Engel, A., S. Goldthwait, U. Passow, and A. Alldredge. 2002. Temporal decoupling of carbon and nitrogen dynamics in a mesocosm diatom bloom. Limnol. Oceanogr. **47**: 753–761. doi:10.4319/lo.2002.47.3.0753

Falk, S., and K. Palmqvist. 1992. Photosynthetic light utilization efficiency, photosystem II heterogeneity, and fluorescence quenching in *Chlamydomonas reinhardtii* during the induction of the CO_2-concentrating mechanism. Plant Physiol **100**: 685–691. doi:10.1104/pp.100.2.685

Feng, Y., and others. 2010. Interactive effects of iron, irradiance and CO_2 on Ross Sea phytoplankton. Deep-Sea Res. Part I Oceanogr. Res. Pap. **57**: 368–383. doi:10.1016/j.dsr.2009.10.013

Flynn, J. F., J. C. Blackford, M. E. Baird, J. A. Raven, D. R. Clark, J. Beardall, C. Brownlee, H. Fabian, and G. L. Wheeler. 2012. Changes in pH at the exterior surface of plankton with ocean acidification. Nat Clim Chang **2**: 510–513. doi:10.1038/nclimate1489

Garibotti, I. A., M. Vernet, R. C. Smith, R. M. Ross, and L. B. Quetin. 2003. Phytoplankton spatial distribution patterns along the Western Antarctic Peninsula (Southern Ocean). Mar. Ecol. Progr. Ser. **261**: 21–39. doi:10.3354/meps261021

Garibotti, I. A., M. Vernet, R. C. Smith, and M. E. Ferrario. 2005. Interannual variability in the distribution of the phytoplankton standing stock across the seasonal sea-ice zone west of the Antarctic Peninsula. J. Plankton Res. **27**: 825–843. doi:10.1093/plankt/fbi056

Genty, B., J.-M. Briantais, and N. R. Baker. 1989. The relationship between the quantum yield of photosynthetic electron transport and quenching of chlorophyll fluorescence. Biochim. Biophys. Acta **990**: 87–92. doi:10.1016/S0304-4165(89)80016-9

Grasshoff, K., M. Ehrhardt, and K. Kremling. 1983. Methods of seawater analysis. Verlag Chemie GmbH.

Hancock, A. M., A. T. Davidson, J. McKinlay, A. McMinn, K. Schulz, and R. L. van den Enden. 2018. Ocean acidification changes the structure of an Antarctic coastal protistan community. Biogeosciences **15**: 2393–2410. doi:10.5194/bg-15-2393-2018

Heber, U., H. Egneus, U. Hanck, M. Jensen, and S. Koster. 1978. Regulation of photosynthetic electron-transport and photophosphorylation in intact chloroplasts and leaves of *Spinacia oleracea* L. Planta **143**: 41–49. doi:10.1007/BF00389050

Heiden, J. P., K. Bischof, and S. Trimborn. 2016. Light intensity modulates the response of two Antarctic diatom species to ocean acidification. Front. Mar. Sci. **3**: 1–17. doi:10.3389/fmars.2016.00260

Heiden, J. P., S. Thoms, K. Bischof, and S. Trimborn. 2018. Ocean acidification stimulates particulate organic carbon accumulation in two Antarctic diatom species under moderate and high solar radiation. J. Phycol. **54**: 505–517. doi:10.1111/jpy.12753

Henley, S. F., R. E. Tuerena, A. L. Annett, A. E. Fallick, M. P. Meredith, H. J. Venables, A. Clarke, and R. S. Ganeshram. 2017. Macronutrient supply, uptake and recycling in the coastal ocean of the west Antarctic Peninsula. Deep-Sea Res. Part II Top. Stud. Oceanogr. **139**: 58–76. doi:10.1016/j.dsr2.2016.10.003

Hoogstraten, A., M. Peters, K. R. Timmermans, and H. J. W. de Baar. 2012*a*. Combined effects of inorganic carbon and light on *Phaeocystis globosa* Scherffel (Prymnesiophyceae). Biogeosciences **9**: 1885–1896. doi:10.5194/bg-9-1885-2012

Hoogstraten, A., K. R. Timmermans, and H. J. W. de Baar. 2012*b*. Morphological and physiological effects in *Proboscia alata* (Bacillariophyceae) grown under different light and CO_2 conditions of the modern Southern Ocean. J. Phycol. **48**: 559–568. doi:10.1111/j.1529-8817.2012.01148.x

Hoppe, C. J. M., C. S. Hassler, C. D. Payne, P. D. Tortell, B. R. Rost, and S. Trimborn. 2013. Iron limitation modulates ocean acidification effects on Southern Ocean phytoplankton communities. PLoS One **8**: e79890. doi:10.1371/journal.pone.0079890

Hoppe, C. J. M., L. Holtz, S. Trimborn, and B. Rost. 2015. Ocean acidification decreases the light-use efficiency in an Antarctic diatom under dynamic but not constant light. New Phytol. **207**: 159–171. doi:10.1111/nph.13334

Hyewon, K., et al. 2018. Inter-decadal variability of phytoplankton biomass along the coastal West Antarctic Peninsula. Philos Trans A Math Phys Eng Sci. **376**: 2122. doi:10.1098/rsta.2017.0174

IPCC. 2014. Climate change 2014: Synthesis report. *In* R. K. Pachauri and L. A. Meyer [eds.], Contribution of working groups I, II and III to the fifth assessment report of the Intergovernmental Panel on Climate Change. IPCC.

Jones, E. M., M. Fenton, M. P. Meredith, N. M. Clargo, S. Ossebaar, H. W. Ducklow, H. J. Venables, and H. J. W. de Baar. 2017.

Ocean acidification and calcium carbonate saturation states in the coastal zone of the West Antarctic Peninsula. Deep-Sea Res. Part II Top. Stud. Oceanogr. **139**: 181–194. doi:10.1016/j.dsr2.2017.01.007

Koch, F., S. Beszteri, L. Harms, and S. Trimborn. 2019. The impacts of iron limitation and ocean acidification on the cellular stoichiometry, photophysiology and transcriptome of *Phaeocystis antarctica*. Limnol Oceanogr. **64**: 357–375. doi:10.1002/lno.11045

Kolber, Z. S., O. Prášil, and P. G. Falkowski. 1998. Measurements of variable chlorophyll fluorescence using fast repetition rate techniques: Defining methodology and experimental protocols. Biochim. Biophys. Acta **1367**: 88–106. doi:10.1016/S0005-2728(98)00135-2

Kulk, G., W. H. van de Poll, and A. G. J. Buma. 2018. Photophysiology of nitrate limited phytoplankton communities in Kongsfjorden, Spitsbergen. Limnol. Oceanogr. **63**: 2606–2617. doi:10.10002/lno.10963.

Lancelot, C., and S. Mathot. 1987. Dynamics of a *Phaeocystis*-dominated spring bloom in Belgian coastal waters. I. Phytoplanktonic activities and related parameters. Mar. Ecol. Progr. Ser. **37**: 249–257.

Legge, O. J., D. C. E. Bakker, M. T. Johnson, M. P. Meredith, H. J. Venables, P. J. Brown, and G. A. Lee. 2015. The seasonal cycle of ocean-atmosphere CO_2 flux in Ryder Bay, West Antarctic Peninsula. Geophys. Res. Lett. **42**: 2934–2942. doi:10.1002/2015GL063796

Li, W., K. Gao, and J. Beardall. 2012. Interactive effects of ocean acidification and nitrogen-limitation on the diatom *Phaeodactylum tricornutum*. PLoS One **7**: 1–8. doi:10.1371/journal.pone.0051590

Mathot, S., W. O. Smith, C. A. Carlson, D. L. Garrison, M. M. Gowing, and C. L. Vickers. 2000. Carbon partitioning within *Phaeocystis antarctica* (Prymnesiophyceae) colonies in the Ross Sea, Antarctica. J. Phycol. **36**: 1049–1056. doi:10.1046/j.1529-8817.2000.99078.x

McMinn, A., M. N. Müller, A. Martin, and K. G. Ryan. 2014. The response of Antarctic sea ice algae to changes in pH and CO_2. PLoS One **9**: e86984. doi:10.1371/journal.pone.0086984

Mehrbach, C., C. H. Culberson, J. E. Hawley, and R. M. Pytkowicz. 1973. Measurement of the apparent dissociation constants of carbonic acid in seawater at atmospheric pressure. Limnol. Oceanogr. **18**: 897–907. doi:10.4319/lo.1973.18.6.0897

Meredith, M. P., and J. C. King. 2005. Rapid climate change in the ocean west of the Antarctic Peninsula during the second half of the 20th century. Geophys. Res. Lett. **32**: L19604. doi:10.1029/2005GL024042

Moisan, T. A., and B. G. Mitchell. 1999. Photophysiological acclimation of *Phaeocystis antarctica* Karsten under light limitation. Limnol. Oceanogr. **44**: 247–258. doi:10.4319/lo.1999.44.2.0247

Moline, M. A., H. Claustre, T. K. Frazer, O. Schofield, and M. Vernet. 2004. Alteration of the food web along the Antarctic Peninsula in response to a regional warming trend. Glob. Chang. Biol. **10**: 1973–1980. doi:10.1111/j.1365-2486.2004.00825.x

Montes-Hugo, M., S. C. Doney, H. W. Ducklow, W. Fraser, D. Martinson, S. E. Stammerjohn, and O. Schofield. 2009. Recent changes in phytoplankton communities associated with rapid regional climate change along the Western Antarctic Peninsula. Science **323**: 1470–1473. doi:10.1126/science.1164533

Murphy, J., and J. P. Riley. 1962. A modified single solution method for the determination of phosphate in natural waters. Anal. Chim. Acta **27**: 31–36. doi:10.1016/S0003-2670(00)88444-5

Orr, J. C., and others. 2005. Anthropogenic ocean acidification over the twenty-first century and its impact on calcifying organisms. Nature **437**: 681–686. doi:10.1038/nature04095

Oxborough, K., C. M. Moore, D. J. Suggett, T. Lawson, H. G. Chan, and R. J. Geider. 2012. Direct estimation of functional PSII reaction center concentration and PSII electron flux on a volume basis: A new approach to the analysis of Fast Repetition Rate fluorometry (FRRf) data. Limnol. Oceanogr.: Methods **10**: 142–154. doi:10.4319/lom.2012.10.142

Palmisano, A. C., J. B. Soohoo, S. L. Soohoo, S. T. Kottmeier, L. L. Craft, and C. W. Sullivan. 1986. Photoadaptation in *Phaeocystis pouchetii* advected beneath annual sea ice in McMurdo Sound, Antarctica. J. Plankton Res. **8**: 891–906. doi:10.1093/plankt/8.5.891

Peperzak, L. 1993. Daily irradiance governs growth rates and colony formation of *Phaeocystis* (Prymnesiophyceae). J. Plankton Res. **15**: 809–821. doi:10.1093/plankt/15.7.809

Perl, J. 2009. The SDSU (CHORS) method, p. 89–90. *In* S. B. Hooker and others. [eds.], The third SeaWiFS HPLC analysis round-robin experiment (SeaHARRE-3). NASA Goddard Space Flight Center.

Pierrot, D., E. Lewis, and D. W. R. Wallace. 2006. MS Excel program developed for CO_2 system calculations. ORNL/CDIAC-105a. Carbon Dioxide Information Analysis Center, Oak Ridge National Laboratory, US Department of Energy.

Ralph, P. J., and R. Gademann. 2005. Rapid light curves: A powerful tool to assess photosynthetic activity. Aquat. Bot. **82**: 222–237. doi:10.1016/j.aquabot.2005.02.006

Riegman, R., and W. von Boekel. 1996. The ecophysiology of *Phaeocystis globosa*: A review. J. Sea Res. **35**: 235–242. doi:10.1016/S1385-1101(96)90750-9

Rozema, P. D., G. Kulk, M. P. Veldhuis, A. G. J. Buma, M. P. Meredith, and W. H. van de Poll. 2017*a*. Interannual variability in phytoplankton biomass and species composition in northern Marguerite Bay (West Antarctic Peninsula) is governed by both winter sea ice cover and summer stratification. Limnol. Oceanogr. **62**: 235–252. doi:10.1002/lno.10391

Rozema, P. D., H. J. Venables, W. H. van de Poll, A. Clarke, M. P. Meredith, and A. G. J. Buma. 2017*b*. Assessing drivers

of coastal primary production in northern Marguerite Bay, Antarctica. Front. Mar. Sci. **4**: 184. doi:10.3389/fmars.2017.00184

Schulz, K. G., and others. 2017. Phytoplankton blooms at increasing levels of atmospheric carbon dioxide: Experimental evidence for negative effects on prymnesiophytes and positive on small picoeukaryotes. Front. Mar. Sci. **4**: 64. doi:10.3389/fmars.2017.00064

Shields, A. R., and W. O. Smith. 2009. Size-fractionated photosynthesis/irradiance relationships during *Phaeocystis antarctica* dominated blooms in the Ross Sea, Antarctica. J. Plankton Res. **31**: 709–712. doi:10.1093/plankt/fbp022

Smith, W. O., and V. L. Asper. 2001. The influence of phytoplankton assemblage composition on biogeochemical characteristics and cycles in the southern Ross Sea, Antarctica. Deep-Sea Res. Part I Oceanogr. Res. Pap. **48**: 137–161. doi:10.1016/S0967-0637(00)00045-5

Su, W., T. Jakob, and C. Wilhelm. 2012. The impact of nonphotochemical quenching of fluorescence on the photon balance in diatoms under dynamic light conditions. J. Phycol. **48**: 336–346. doi:10.1111/j.1529-8817.2012.01128.x

Suggett, D. J., H. L. MacIntyre, and R. J. Geider. 2004. Evaluation of biophysical and optical determinations of light absorption by photosystem II in phytoplankton. Limnol. Oceanogr.: Methods **2**: 316–332. doi:10.4319/lom.2004.2.316

Suggett, D. J., C. M. Moore, A. E. Hickman, and R. J. Geider. 2009. Interpretation of fast repetition rate (FRR) fluorescence: Signatures of phytoplankton community structure versus physiological state. Mar. Ecol. Progr. Ser. **376**: 1–19. doi:10.3354/meps07830

Sweeney, C., D. A. Hansell, C. A. Carlson, L. A. Codispoti, L. L. Gordon, J. Marra, F. J. Millero, W. O. Smith, and T. Takahashi. 2000. Biogeochemical regimes, net community production and carbon export in the Ross Sea, Antarctica. Deep-Sea Res. Part II Top. Stud. Oceanogr. **47**: 3369–3394. doi:10.1016/S0967-0645(00)00072-2

Taucher, J., K. G. Schulz, T. Dittmar, U. Sommer, A. Oschlies, and U. Riebesell. 2012. Enhanced carbon overconsumption in response to increasing temperatures during a mesocosm experiment. Biogeosciences **9**: 3531–3545. doi:10.5194/bg-9-3531-2012

Thoisen, C., K. Riisgaard, N. Lundholm, T. G. Nielsen, and P. J. Hansen. 2015. Effect of acidification on an Arctic phytoplankton community from Disko Bay, West Greenland. Mar. Ecol. Progr. Ser. **520**: 21–34. doi:10.3354/meps11123

Thomas, C. R., G. R. Hasle, E. E. Syvertsen, K. A. Steidinger, K. Tangen, J. Throndsten, and B. R. Heimdal. 1997. Identifying marine phytoplankton. Academic press.

Thomson, P., A. Davidson, and L. Maher. 2016. Increasing CO_2 changes community composition of pico- and nano-sized protists and prokaryotes at a coastal Antarctic site. Mar. Ecol. Progr. Ser. **554**: 51–69. doi:10.3354/meps11803

Toggweiler, J. 1994. Vanishing in Bermuda. Nature **372**: 505–506. doi:10.1038/372505a0

Tortell, P. D., G. R. DiTullio, D. M. Sigman, and F. M. M. Morel. 2002. CO_2 effects on taxonomic composition and nutrient utilization in an Equatorial Pacific phytoplankton assemblage. Mar. Ecol. Progr. Ser. **236**: 37–43. doi:10.3354/meps236037

Tortell, P. D., et al. 2008. CO_2 sensitivity of Southern Ocean phytoplankton. Geophys. Res. Lett. **35**: 1–5. doi:10.1029/2007GL032583

Tréguer, P. 2002. Silica and the cycle of carbon in the ocean. Geoscience **334**: 3–11. doi:10.1016/S1631-0713(02)01680-2

Trimborn, S., T. Brenneis, E. Sweet, and B. Rost. 2013. Sensitivity of Antarctic phytoplankton species to ocean acidification: Growth, carbon acquisition, and species interaction. Limnol. Oceanogr. **58**: 997–1007. doi:10.4319/lo.2013.58.3.0997

Trimborn, S., C. J. M. Hoppe, B. B. Taylor, A. Bracher, and C. S. Hassler. 2015. Physiological characteristics of open ocean and coastal phytoplankton communities of Western Antarctic Peninsula and Drake Passage waters. Deep-Sea Res. Part I Oceanogr. Res. Pap. **98**: 115–124. doi:10.1016/j.dsr.2014.12.010

Trimborn, S., S. Thoms, T. Brenneis, J. P. Heiden, S. Beszteri, and K. Bischof. 2017*a*. Two Southern Ocean diatoms are more sensitive to ocean acidification and changes in irradiance than the prymnesiophyte *Phaeocystis antarctica*. Physiol. Plant. **160**: 155–170. doi:10.1111/ppl.12539

Trimborn, S., T. Brenneis, C. J. M. Hoppe, L. Norman, J. Santos, L. Laglera, D. Wolf-Gladrow, and C. Hassler. 2017*b*. Iron sources alter the response of Southern Ocean phytoplankton to ocean acidification. Mar. Ecol. Prog. Ser. **578**: 35–50. doi:10.3354/meps12250

Turner, J., T. Maksym, T. Phillips, G. J. Marshall, and M. P. Meredith. 2013. The impact of changes in sea ice advance on the large winter warming on the Western Antarctic Peninsula. Int. J. Climatol. **33**: 852–861. doi:10.1002/joc.3474

Utermöhl, H. 1958. Zur Vervollkommnung der quantitativen Phytoplankton-Methodik. Mitt. Int. Ver. Theor. Angew. Limnol. **9**: 1–38.

van de Poll, W. H., M. Lagunas, T. de Vries, R. J. W. Visser, and A. G. J. Buma. 2011. Non-photochemical quenching of chlorophyll fluorescence and xanthophyll cycle responses after excess PAR and UVR in *Chaetoceros brevis*, *Phaeocystis antarctica* and coastal Antarctic phytoplankton. Mar Ecol Prog Ser **426**: 119–131. doi:10.3354/meps09000

van de Poll, W. H., G. Kulk, P. D. Rozema, C. P. D. Brussaard, R. J. W. Visser, and A. G. J. Buma. 2018. Contrasting glacial meltwater effects on post-bloom phytoplankton on temporal and spatial scales in Kongsfjorden, Spitsbergen. Elem. Sci. Anth. **6**: 50. doi:10.1525/elementa.307

Van Heukelem, L., and C. S. Thomas. 2001. Computer-assisted high-performance liquid chromatography method development with applications to the isolation and analysis of phytoplankton pigments. J. Chromatogr. A **910**: 31–49. doi:10.1016/S0378-4347(00)00603-4

Veldhuis, M. J. W., and W. Admiraal. 1987. Influence of phosphate depletion on the growth and colony formation of *Phaeocystis pouchetii*. Mar. Biol. **95**: 47–54. doi:10.1007/BF00447484

Venables, H. J., A. Clarke, and M. P. Meredith. 2013. Wintertime controls on summer stratification and productivity at the Western Antarctic Peninsula. Limnol. Oceanogr. **58**: 1035–1047. doi:10.4319/lo.2013.58.3.1035

Verity, P. G., S. J. Whipple, J. C. Nejstgaard, and A.-C. Alderkamp. 2007. Colony size, cell number, carbon and nitrogen contents of *Phaeocystis pouchetii* from western Norway. J. Plankton Res. **29**: 359–367. doi:10.1093/plankt/fbm021

Vernet, M., D. Martinson, R. Iannuzzi, S. Stammerjohn, W. Kozlowski, K. Sines, R. Smith, and I. Garibotti. 2008. Primary production within the sea-ice zone west of the Antarctic Peninsula: I—sea ice, summer mixed layer, and irradiance. Deep-Sea Res. Part II Top. Stud. Oceanogr. **55**: 2068–2085. doi:10.1016/j.dsr2.2008.05.021

Wagner, H., T. Jakob, and C. Wilhelm. 2006. Balancing the energy flow from captured light to biomass under fluctuating light conditions. New Phytol. **169**: 95–108. doi:10.1111/j.1469-8137.2005.01550.x

Wang, X., Y. Wang, and W. O. Smith. 2011. The role of nitrogen on the growth and colony development of *Phaeocystis globosa* (Prymnesiophyceae). Eur J. Phycol. **46**: 305–314. doi:10.1080/09670262.2011.602430

Young, J. N., S. A. Kranz, J. A. L. Goldman, P. D. Tortell, and F. M. M. Morel. 2015. Antarctic phytoplankton down-regulate their carbon-concentrating mechanisms under high CO_2 with no change in growth rates. Mar. Ecol. Progr. Ser. **532**: 13–28. doi:10.3354/meps11336

Zeebe, R. E., and D. A. Wolf-Gladrow. 2001. CO_2 in seawater: Equilibrium, kinetics, isotopes. Gulf Professional Publishing.

Zuur, A., E. N. Ieno, and G. M. Smith. 2007. Analyzing ecological data. Springer Science & Business Media.

Acknowledgments

The authors gratefully acknowledge the Bristish Antarctic Survey (BAS), the Royal Netherlands institute for Sea Research (NIOZ), and the Netherlands Organisation for Scientific Research (NWO) for the opportunity to conduct fieldwork at the Dierck Gerritz and Bonner laboratories at Rothera. The RaTS long-term monitoring program is a component of the Polar Oceans research program at BAS, funded by the Natural Environment Research Council (NERC). The work of JPH, CV, and ST was funded by the Helmholtz association (Young Investigator Group EcoTrace, VH-NG-901). This work is part of postdoctoral research (E. Jones) at the University of Groningen under the research programme 866.13.006, which is (partly) financed by the Netherlands Polar Programme at NWO.

Conflict of Interest

None declared.

Submitted 31 July 2018
Revised 28 November 2018
Accepted 28 January 2019

Associate editor: Heidi Sosik